

UMN–TH–3432/15

FTPI–MINN–15/19

April 2015

## Big Bang Nucleosynthesis: 2015

Richard H. Cyburt

*Joint Institute for Nuclear Astrophysics (JINA),  
National Superconducting Cyclotron Laboratory (NSCL),  
Michigan State University, East Lansing, MI 48824*

Brian D. Fields

*Departments of Astronomy and of Physics,  
University of Illinois, Urbana, IL 61801*

Keith A. Olive

*William I. Fine Theoretical Physics Institute, School of Physics and Astronomy,  
University of Minnesota, Minneapolis, MN 55455, USA*

Tsung-Han Yeh

*Departments of Astronomy and of Physics,  
University of Illinois, Urbana, IL 61801*

## Abstract

Big-bang nucleosynthesis (BBN) describes the production of the lightest nuclides via a dynamic interplay among the four fundamental forces during the first seconds of cosmic time. We briefly overview the essentials of this physics, and present new calculations of light element abundances through  ${}^6\text{Li}$  and  ${}^7\text{Li}$ , with updated nuclear reactions and uncertainties including those in the neutron lifetime. We provide fits to these results as a function of baryon density and of the number of neutrino flavors,  $N_\nu$ . We review recent developments in BBN, particularly new, precision *Planck* cosmic microwave background (CMB) measurements that now probe the baryon density, helium content, and the effective number of degrees of freedom,  $N_{\text{eff}}$ . These measurements allow for a tight test of BBN and of cosmology using CMB data alone. Our likelihood analysis convolves the 2015 *Planck* data chains with our BBN output and observational data. Adding astronomical measurements of light elements strengthens the power of BBN. We include a new determination of the primordial helium abundance in our likelihood analysis. New D/H observations are now more precise than the corresponding theoretical predictions, and are consistent with the Standard Model and the *Planck* baryon density. Moreover, D/H now provides a tight measurement of  $N_\nu$  when combined with the CMB baryon density, and provides a  $2\sigma$  upper limit  $N_\nu < 3.2$ . The new precision of the CMB and of D/H observations together leave D/H predictions as the largest source of uncertainties. Future improvement in BBN calculations will therefore rely on improved nuclear cross section data. In contrast with D/H and  ${}^4\text{He}$ ,  ${}^7\text{Li}$  predictions continue to disagree with observations, perhaps pointing to new physics. We conclude with a look at future directions including key nuclear reactions, astronomical observations, and theoretical issues.

## I. INTRODUCTION

Big bang nucleosynthesis (BBN) is one of few probes of the very early Universe with direct experimental or observational consequences [1–3]. In the context of the Standard Models of cosmology and of nuclear and particle physics, BBN is an effectively parameter-free theory [5]. Namely, standard BBN (SBBN) assumes spacetime characterized by General Relativity and the  $\Lambda$ CDM cosmology, and microphysics characterized by Standard Model particle content and interactions, with three light neutrino species, with negligible effects due to dark matter and dark energy.

In SBBN, the abundances of the four light nuclei are usually parameterized by the baryon-to-photon ratio  $\eta \equiv n_b/n_\gamma$ , or equivalently the present baryon density,  $\Omega_b h^2 \equiv \omega_b$ . This quantity has been fixed by a series of precise measurements of microwave background anisotropies, most recently by *Planck* yielding  $\eta = 6.10 \pm 0.04$  [6]. Thus the success or failure of SBBN rests solely on the comparison of theoretical predictions with observational determinations.

While precise predictions from SBBN are feasible, they rely on well-measured cross sections and a well-measured neutron lifetime. Indeed, even prior to the *WMAP* era, theoretical predictions for D,  $^3\text{He}$ , and  $^4\text{He}$  were reasonably accurate, however, uncertainties in nuclear cross sections leading to  $^7\text{Be}$  and  $^7\text{Li}$  were relatively large. Many modern analyses of nuclear rates for BBN were based on the NACRE compilation [7] and recent BBN calculations by several groups are in good agreement [8–17]. Recent remeasurements of the  $^3\text{He}(\alpha, \gamma)^7\text{Be}$  cross section [18] did improve the theoretical accuracy of the prediction but exacerbated the discrepancy between theory and observation [19]. Very recently, the NACRE collaboration has issued an update (NACRE-II) of its nuclear rate tabulation [20]. These were first used in [21] and we incorporate the new rates in the results discussed below.

The neutron mean life has had a rather sordid history. Because it scales the weak interaction rates between  $n \leftrightarrow p$ , the neutron mean life controls the neutron-to-proton ratio at freeze-out and directly affects the  $^4\text{He}$  abundance (and the other light elements to a lesser extent). The value  $\tau_n = 918 \pm 14$  s reported by Cristensen et al. in 1972 [22] dominated the weighted mean for the accepted value through mid 1980s. Despite the low value of  $877 \pm 8$  s reported by Bondarenko et al. in 1978 [23], the ‘accepted’ mean value (as reported in the “Review of Particle Physics”) remained high, and the high value was reinforced by a measurement by Byrne et al. [24] in 1980 of  $937 \pm 18$  s. The range 877 s - 937 s was

used by Olive et al. [25] to explore the sensitivity of BBN predictions to this apparently uncertain quantity treated then as an uncertain input parameter to BBN calculations (along with the number of light neutrino flavors  $N_\nu$  and the baryon-to-photon ration,  $\eta$ ). In the late 1980's a number of lower measurements began to surface, and in 1989 Mampe et al. [26] claimed to measure a mean life of  $877.6 \pm 3$  s (remarkably consistent with the current world average). Subsequently, it appeared that questions regarding the neutron mean life had been resolved, as the mean value varied very little between 1990 and 2010, settling at  $885.6 \pm 0.8$ . However, in 2005, there was already a sign that the mean life was about to shift to lower values once again. Serebrov et al. [27] reported a very precise measurement of  $878.5 \pm 0.8$  which was used in BBN calculations in [28]. This was followed by several more recent measurements and reanalyses tending to lower values so that the current world average is [29]  $\tau_n = 880.3 \pm 1.1$ . We will explore the impact of the new lifetime on the light element abundances.

On the observational side, the  $^4\text{He}$  abundance determination comes most directly from measurements of emission lines in highly ionized gas in nearby low-metallicity dwarf galaxies (extragalactic HII regions). The helium abundance uncertainties are dominated by systematic effects [30–32]. The model used to determine the  $^4\text{He}$  abundance contains eight physical parameters, including the  $^4\text{He}$  abundance, that is used to predict a set of ten H and He emission line ratios, which can be compared with observations [33–36]. Unfortunately, there are only a dozen or so observations for which the data and/or model is reliable, and even in those cases, degeneracies among the parameters often lead to relatively large uncertainties for each system as well as a large uncertainty in the regression to zero metallicity. Newly calculated  $^4\text{He}$  emissivities [37] and the addition of a new near infra-red line [36] have led to lower abundance determinations [38, 39], bringing the central value of the  $^4\text{He}$  abundance determination into good agreement with the SBBN prediction. Moreover, *Planck* measurements of CMB anisotropies are now precise enough to give interesting measures of primordial helium via its effect on the anisotropy damping tail.

New observations and analyses of quasar absorption systems have dramatically improved the observational determination of D/H. Using a handful of systems where accurate determinations can be made, Cooke et al. [40] not only significantly lowered the uncertainty in the mean D/H abundance, but the dispersion present in old data has all but been erased. Because of its sensitivity to the baryon density, D/H is a powerful probe of SBBN and

now the small uncertainties in both the data and prediction become an excellent test of concordance between SBBN and the CMB determination of the baryon density.

In contrast to the predicted abundances of  $^4\text{He}$  and  $\text{D}/\text{H}$ , the  $^7\text{Li}$  abundance shows a definite discrepancy with all observational determinations from halo dwarf stars. To date, there is no solution that is either not tuned or requires substantial departures from Standard Model physics. Attempts at solutions include modifications of the nuclear rates [17, 41, 42] or the inclusion of new resonant interactions [43–45]; stellar depletion [46]; lithium diffusion in the post-recombination universe [47]; new (non-standard model) particles decaying around the time of BBN [48–51]; axion cooling [52]; or variations in the fundamental constants [53, 54].

In this review, we survey the current status of SBBN theory and its compatibility with observation. Using an up-to-date nuclear network, we present new Monte-Carlo estimates of the theoretical predictions based on a full set of nuclear cross sections and their uncertainties. We will highlight those reactions that still carry the greatest uncertainties and how those rates affect the light element abundances. We will also highlight the effect of the new determination of the neutron mean life on the  $^4\text{He}$  abundance and the abundances of the other light elements as well.

Compatibility with observation is demonstrated by the construction of likelihood functions for each of the light elements [10] by convolving individual theoretical and observational likelihood functions. Our BBN calculations are also convolved with data chains provided by the 2015 *Planck* data release [6]. This allows us to construct 2-dimensional  $(\eta, Y_p)$  and 3-dimensional  $(\eta, Y_p, N_\nu)$  likelihood distributions. Such an analysis is timely and important given the recent advances in the  $^4\text{He}$  and  $\text{D}/\text{H}$  observational landscape. In fact, despite the accuracy of the SBBN prediction for  $\text{D}/\text{H}$ , the tiny uncertainty in observed  $\text{D}/\text{H}$  now leads to a likelihood dominated by theory errors. The tight agreement between  $\text{D}/\text{H}$  prediction and observation is in sharp contrast to the discrepancy in  $^7\text{Li}/\text{H}$ . We briefly discuss this “lithium problem,” and discuss recent nuclear measurements that rule out a nuclear fix to this problem, leaving as explanations either astrophysical systematics or new physics. While the  $^6\text{Li}$  was shown to be an artifact of astrophysical systematics [55, 56], for now, the  $^7\text{Li}$  problem persists.

As a tool for modern cosmology and astro-particle physics, SBBN is a powerful probe for constraining physics beyond the Standard Model [57]. Often, these constraints can be

parameterized by the effect of new physics on the speed-up of the expansion rate of the Universe and subsequently translated into a limit on the number of equivalent neutrino flavors or effective number of relativistic degrees of freedom,  $N_{\text{eff}}$ . We update these constraints and compare them to recent limits on  $N_{\text{eff}}$  from the microwave background anisotropy and large scale structure. We will show that for the first time, D/H provides a more stringent constraint on  $N_{\text{eff}}$  than the  $^4\text{He}$  mass fraction.

The structure of this review is as follows: In the next section, we discuss the relevant updates to the nuclear rates used in the calculation of the light element abundances. We also discuss the sensitivity to the neutron mean life. In this section, we present our baseline results for SBBN assuming the *Planck* value for  $\eta$ , the RPP value for  $\tau_n$  and  $N_\nu = 3$ . In section III, we briefly review the values of the observational abundance determinations and their uncertainties that we adopt for comparison with the SBBN calculations from the previous section. In section IV, we discuss our Monte Carlo methods, and construct likelihood functions for each of the light elements, and we extend these methods to discuss limits on  $N_\nu$  in section V. The lithium problem is summarized in section VI. A discussion of these results and the future outlook appears in section VII.

## II. PRELIMINARIES

### A. SBBN

As defined in the previous section, SBBN refers to BBN in the context of Einstein gravity, with a Friedmann-Lemaître-Robertson-Walker cosmological background. It assumes the Standard Model of nuclear and particle physics, or in other words, the standard set of nuclear and particle interactions and nuclear and particle content. Implicitly, this means a theory with a number  $N_\nu = 3$  of very light neutrino flavors<sup>1</sup>. SBBN also makes the well-justified assumption that during the epoch of nucleosynthesis, the universe was radiation dominated, so that the dominant component of the energy density of the universe can be

---

<sup>1</sup> We distinguish between the number of neutrino flavors, three in the Standard Model, and  $N_{\text{eff}}$ , equal to 3.046 in the Standard Model, which corresponds to the effective number of neutrinos present in the thermal bath due to the higher temperature from  $e^+e^-$  annihilations before neutrinos are completely decoupled.

expressed as

$$\rho = \frac{\pi^2}{30} \left( 2 + \frac{7}{2} + \frac{7}{4} N_\nu \right) T^4, \quad (1)$$

taking into account the contributions of photons, electrons and positrons, and neutrino flavors appropriate for temperatures  $T > 1$  MeV. At these temperatures, weak interaction rates between neutrons and protons maintain equilibrium.

At lower temperatures, the weak interactions can no longer keep up with the expansion of the universe or equivalently, the mean time for an interaction becomes longer than the age of the Universe. Thus, the freeze-out condition is set by

$$G_F^2 T^5 \sim \Gamma_{\text{wk}}(T_f) = H(T_f) \sim G_N^{1/2} T^2, \quad (2)$$

where  $\Gamma_{\text{wk}}$  represents the relevant weak interaction rates per baryon that scale roughly as  $T^5$ , and  $H$  is the Hubble parameter

$$H^2 = \frac{8\pi}{3} G_N \rho \quad (3)$$

and scales as  $T^2$  in a radiation dominated universe.  $G_F$  and  $G_N$  are the Fermi and Newton constants respectively. Freeze-out occurs when the weak interaction rate falls below the expansion rate,  $\Gamma_{\text{wk}} < H$ . The  $\beta$ -interactions that control the relative abundances of neutrons and protons freeze out at  $T_f \sim 0.8$  MeV. At freeze-out, the neutron-to-proton ratio is given approximately by the Boltzmann factor,  $(n/p)_f \simeq e^{-\Delta m/T_f} \sim 1/5$ , where  $\Delta m = m_n - m_p$  is the neutron-proton mass difference. After freeze-out, free neutron decays drop the ratio slightly to  $(n/p)_{\text{bbn}} \simeq 1/7$  before nucleosynthesis begins. A useful semi-analytic description of freeze-out can be found in [58, 59].

The first link in the nucleosynthetic chain is  $p + n \rightarrow d + \gamma$  and although the binding energy of deuterium is relatively small,  $E_B = 2.2$  MeV, the large number of photons relative to nucleons,  $\eta^{-1} \sim 10^9$  causes the so-called deuterium bottleneck. BBN is delayed until  $\eta^{-1} \exp(-E_B/T) \sim 1$  when the deuterium destruction rate finally falls below its production rate. This occurs when the temperature is approximately  $T \sim E_B / \ln \eta^{-1} \sim 0.1$  MeV.

To a good approximation, almost all of the neutrons present when the deuterium bottleneck breaks end up in  $^4\text{He}$ . It is therefore very easy to estimate the  $^4\text{He}$  mass fraction,

$$Y_p = \frac{2(n/p)}{1 + (n/p)} \approx 0.25, \quad (4)$$

where we have evaluated  $Y_p$  using  $(n/p) \approx 1/7$ . The other light elements are produced in significantly smaller abundances, justifying our approximation for the  $^4\text{He}$  mass fraction. D and  $^3\text{He}$  are produced at the level of about  $10^{-5}$  by number, and  $^7\text{Li}$  at the level of  $10^{-10}$  by number. A cooling Universe, Coulomb barriers, and the mass gap at  $A = 8$  prevents the production of other isotopes in any significant quantity.

## B. Updated Nuclear Rates

Our BBN results use an updated version of our code [10, 19], itself a descendant of the Wagoner code [60]. For the weak  $n \leftrightarrow p$  interconversion rates, the code calculates the 1-D phase space integrals at tree level; this corresponds to the assumption that the nucleon remains at rest. The weak  $n \leftrightarrow p$  interconversion rates are normalized such that we recover the adopted mean neutron lifetime at low temperature and density. To this we added order- $\alpha$  radiative and bremsstrahlung QED corrections, and included Coulomb corrections for reactions with  $pe^-$  in the initial or final states [61]. We neglected additional corrections, because the overall contribution of all other effects is relatively insignificant. Finite temperature radiative corrections leads to  $\Delta Y_p \sim 0.0004$ ; corrections to electron mass leads to  $\Delta Y_p \sim -0.0001$ ; neutrino heating due to  $e^+e^-$  annihilation leads to  $\Delta Y_p \sim 0.0002$  [61]. Problems in the original code due to the choice of time-steps in the numerical integration [62] have been corrected here. Finally, we included the effects of finite nucleon mass [63] by increasing the final  $^4\text{He}$  abundance with  $\Delta Y_p = +0.0012$ . We formally adopt the Particle Data Group’s current recommended value [29]:  $\tau_n = 880.3 \pm 1.1$  for the mean free neutron decay lifetime, and assume it is normally distributed.

In addition to the weak  $n \leftrightarrow p$  interconversion rates, BBN relies on well-measured cross sections. The latest update to these reaction rates has been evaluated by the NACRE collaboration and released as NACRE-II [20]. Only charge-induced reactions were considered in NACRE-II, and many more reactions are evaluated there than is relevant for BBN. Those reactions of relevance are shown in table I. The compilation presents tables of reaction rates, with recommended “adopted”, “low” and “high” values. We assume the rates are distributed with a log-normal distribution with:

$$\mu \equiv \ln \sqrt{R_{high} \times R_{low}} \quad (5)$$

$$\sigma \equiv \ln \sqrt{R_{high}/R_{low}}, \quad (6)$$



where  $R_{low}$  and  $R_{high}$  are the recommended “low” and “high” values for the reaction rates, respectively [21]. These rates agree well with previous evaluations [10, 14–16], largely because they depend on the same experimental data. Uncertainties in the NACRE-II evaluation are similar to, but tend to be larger than previous studies. This may stem from the method used to derive accurate descriptions of the data and the fitting potential models used in Distorted-Wave Born Approximation (DWBA) calculations.

TABLE I. Reactions of relevance for BBN from the NACRE-II compilation.

$d(p, \gamma)^3\text{He}$	$d(d, \gamma)^4\text{He}$	$d(d, n)^3\text{He}$
$d(d, p)t$	$t(d, n)^4\text{He}$	$^3\text{He}(d, p)^4\text{He}$
$d(\alpha, \gamma)^6\text{Li}$	$^6\text{Li}(p, \gamma)^7\text{Be}$	$^6\text{Li}(p, \alpha)^3\text{He}$
$^7\text{Li}(p, \alpha)^4\text{He}$	$^7\text{Li}(p, \gamma)^8\text{Be}^a$	

<sup>a</sup>  $^8\text{Be}$  is not in our nuclear network,  $^8\text{Be}$  is assumed to spontaneously decay into  $2^4\text{He}$ 's.

The remaining relevant  $n$ -induced rates,  $p(n, \gamma)d$ ,  $^3\text{He}(n, p)t$  and  $^7\text{Be}(n, p)^7\text{Li}$ , need to be taken from different sources. We adopt the evaluation from [64] for the key reaction  $p(n, \gamma)d$ . The remaining  $(n, p)$  reactions we use are rates taken from [14]. We choose log-normal parameters in such a way to keep the means and variances of the reaction rates invariant.

### C. First Results

As a prelude to the more detailed analysis given below, we first discuss the BBN predictions at a fixed value of  $\eta$ . This benchmark can then be compared to the results of other codes.

Here, we fix  $\eta_{10} \equiv 10^{10}\eta = 6.10$ . This is related to the value of  $\omega_b$  determined by *Planck* [6] based on a combination of temperature and polarization data<sup>2</sup>. The result of our BBN calculation at  $\eta_{10} = 6.10$  can be found in Table II compared to the fit in [3], based on the PArthENoPE code [4]. As one can see, the results of the two codes are in excellent agreement for all of the light elements. The results can be quickly compared with the

<sup>2</sup> A straight interpretation of the *Planck* result based on the TT,TE,EE,+lowP anisotropy data would yield  $\eta_{10} = 6.09$ . However this result already includes the He abundance from BBN. Our choice of  $\eta$  is discussed in Section IV.C and Table IV below.

observed abundances given in the next section. However a more rigorous treatment of the comparison between theory and observation will be given in section IV.

TABLE II. Comparison of BBN Results

	$\eta_{10}$	$N_\nu$	$Y_p$	D/H	$^3\text{He}/\text{H}$	$^7\text{Li}/\text{H}$	$^6\text{Li}/\text{H}$
This Work	6.10	3	0.2470	$2.579 \times 10^{-5}$	$0.9996 \times 10^{-5}$	$4.648 \times 10^{-10}$	$1.288 \times 10^{-14}$
Iocco et al. [3] fit	6.10	3	0.2463	$2.578 \times 10^{-5}$	$0.9983 \times 10^{-5}$	$4.646 \times 10^{-10}$	$1.290 \times 10^{-14}$

### III. OBSERVATIONS

Before making a direct comparison of the SBBN results, we first discuss astrophysical observations of light elements. Here we focus on  $^4\text{He}$ , D, and the Li isotopes, all of which are accessible in primitive environments making it possible to extrapolate existing observations to their primordial abundances. BBN also produces  $^3\text{He}$  in observable amounts, and  $^3\text{He}$  is detectable via its hyperfine emission line, but this line is only accessible within Milky Way gas clouds that are far from pristine [65]. Because of the uncertain post-BBN nucleosynthetic history of  $^3\text{He}$ , it is not possible to use these high-metallicity environments to infer primordial  $^3\text{He}$  at a level useful for probing BBN [66]. After an overview of the observational status of the four remaining isotopes, we turn to the CMB, which includes constraints not only on the baryon density but now also on  $^4\text{He}$  and  $N_{\text{eff}}$ .

#### A. Helium-4

$^4\text{He}$  has long since been the element of choice for setting constraints on physics beyond the Standard Model. The reasoning is simple: as discussed above, the  $^4\text{He}$  abundance is almost completely controlled by the number of free neutrons at the onset of nucleosynthesis, and that number is determined by the freeze-out of the weak  $n \leftrightarrow p$  rates. The resulting mass fraction of  $^4\text{He}$  is given in Eq. (4). As we have seen, the SBBN result for the  $Y_p$  dependence on the baryon density is only logarithmic and therefore  $^4\text{He}$  is not a particularly good baryometer. Nevertheless, it is quite sensitive to any changes in the freeze-out temperature,  $T_f$ , through the relation (2). However, strong limits on physics beyond the Standard Model [57] requires accurate  $^4\text{He}$  abundances from observations.

The  $^4\text{He}$  abundance is determined by measurements of He (and H) emission lines in extragalactic HII regions. Since  $^4\text{He}$  is produced in stars along with heavier elements, the primordial mass fraction of  $^4\text{He}$ ,  $Y_p \equiv \rho(^4\text{He})/\rho_b$ , is determined by a regression of the helium abundance versus metallicity [67]. However, due to numerous systematic uncertainties, obtaining an accuracy better than 1% in the primordial helium abundance is very difficult [30, 34, 68]. The theoretical model that is used to extract a  $^4\text{He}$  abundance contains eight physical parameters to predict the fluxes of nine emission line ratios that can be compared directly with observations <sup>3</sup>. The parameters include, the electron density, optical depth, temperature, equivalent widths of underlying absorption for both H and He, a correction for reddening, the neutral hydrogen fraction, and of course the  $^4\text{He}$  abundance. Using theoretical emissivities, the model can be used to predict the fluxes of 6 He lines (relative to  $\text{H}\beta$ ) as well as 3 H lines (also relative to  $\text{H}\beta$ ). The lines are chosen for their ability to break degeneracies among the inputs when possible. For a recent discussion see [38, 39].

There is a considerable amount of  $^4\text{He}$  data available [33, 34]. A Markov Chain Monte Carlo analysis of the 8-dimensional parameter space for 93 H II regions reported in [34] was performed in [32]. By marginalizing over the other 7 parameters, the  $^4\text{He}$  abundance (and its uncertainty) can be determined. However, for most the data, the  $\chi^2$ s obtained by comparing the theoretically derived fluxes for the 9 emission lines with those observed, were typically very large ( $\gg 1$ ) indicating either a problem with the data, a problem with the model, or problems with both. Selecting only data for which 6 He lines were available, and a  $\chi^2 < 4$ , left only 25 objects for the subsequent analysis. Further cuts of solutions with for example, anomalously high neutral H fractions, or excessive corrections due to underlying absorptions brought the sample down to 14 objects that yielded  $Y = 0.2534 \pm 0.0083 + (54 \pm 102)\text{O}/\text{H}$  based on a linear regression and  $Y_p = 0.2574 \pm 0.0036$  based on a weighted mean of the same data.

Recently, a new analysis of the theoretical emissivities has been performed [37]. This includes improved photoionization cross-sections and a correction of errors found in the previous result. The new emissivities are systematically higher, and for some lines the increase in the emissivity is 3-5% or higher. As a consequence, one expects lower  $^4\text{He}$  abundances using the new emissivities. In [38], the same initial data were used with the

---

<sup>3</sup> Below, we will use results based on the inclusion of a tenth line (seventh He line) seen in the near infra-red [36].

same quality cuts, now leaving 16 objects in the final sample. Individual objects typically showed 5-10 % lower  $^4\text{He}$  abundance yielding  $Y = 0.2465 \pm 0.0097 + (96 \pm 122)\text{O/H}$  for a regression. Once again, one could argue that the lack of true indication of a slope in the data over the restricted baseline may justify using the mean rather than the regression. The mean was then found to be  $Y_p = 0.2535 \pm 0.0036$ . The large errors in  $Y_p$  determined from the regression were due to a combination of large errors on individual objects, a relatively low number of objects with  $\chi^2 < 4$ , a short baseline in O/H, and a poorly determined slope (though the analysis using the new emissivities does show more positive evidence for a slope of Y vs O/H).

More recently, new observations include a near infrared line at  $\lambda 10830$  [36]. The importance of this line stems from its dependence on density and temperature that differs from other observed He lines. This potentially breaks the degeneracy seen between these two parameters that is one of the major culprits for large uncertainties in  $^4\text{He}$  abundance determinations. There are 16 objects satisfying  $\chi^2 \lesssim 6$  [39] (there are now two degrees for freedom rather than one), with all seven He measured (though these are not exactly the same 16 objects used in [38]). Indeed it was found [39] that the inclusion of this line, did in fact reduce the uncertainty and leads to a better defined regression

$$Y_p = 0.2449 \pm 0.0040 + (78.9 \pm 43.3)\text{O/H} \quad (7)$$

Unlike past analyses, there is now a well-defined slope in the regression, making the mean,  $Y_p = 0.2515 \pm 0.0017$  less justifiable as an estimate of primordial  $^4\text{He}$ . The benefit of adding the IR He line is seen to reduce the uncertainty in  $Y_p$  by over a factor of two. This is due to the better determined abundances of individual objects and a better determined slope. It remains the case, however, that most of the available observational data are not well fit by the model. Comparing with the value of  $Y_p$  given in Table II, the intercept of the regression (7) is in good agreement with the results of SBBN.

## B. Deuterium

Because of its strong dependence on the baryon density, deuterium is an excellent baryometer. Furthermore, since there are no known astrophysical sources for deuterium production [69] and thus all deuterium must be of primordial origin, any observed deuterium

provides us with an upper bound on the baryon-to-photon ratio [70, 71]. However, the monotonic decrease in the deuterium abundance over time indicates that the galactic chemical evolution [75, 76] affects the interpretation of any local measurements of the deuterium abundance such as in the local interstellar medium [72], galactic disk [73], or galactic halo [74].

The role of D/H in BBN was significantly promoted when measurements of D/H ratios in quasar absorption systems at high redshift became available. In a short note in 1976, Adams [77] outlined the conditions that would permit the detectability of deuterium in such systems. However it was not until 1997, that the first reliable measurements of D/H at high redshift became available [78] (we do not discuss here the tumultuous period with conflicting high and low measures of D/H). Over the next 20+ years, only a handful of new observations became available with abundances in the range  $D/H = (1 - 4) \times 10^{-5}$  [78, 79]. Despite the fact that there was considerable dispersion in the data (unexpected if these observations correspond to primordial D/H), the weighted mean of the data gave  $D/H = (3.01 \pm 0.21) \times 10^{-5}$  with a sample variance of 0.68. While the data were in reasonably good agreement with the SBBN predicted value (discussed in detail below) using the CMB determined value for the baryon-to-photon ratio, the dispersion indicated that either the quoted error bars were underestimated and larger systematic errors were unaccounted for, or if the dispersion was real, in situ destruction of deuterium must have taken place within these absorbers. In the latter case, the highest ratio ( $\sim 4 \times 10^{-5}$ ) should be taken as the post-BBN value, leaving room for some post-BBN production of D/H that may have accompanied the destruction of  ${}^7\text{Li}$  - we return to this possibility (or lack thereof) below.

In 2012, Pettini and Cooke [80] published results from a new observation of an absorber at  $z = 3.05$ , with  $D/H = (2.54 \pm 0.05) \times 10^{-5}$  corresponding to an uncertainty of about 2% that can be compared with typical uncertainties of 10 – 20 % in previous observations. This was followed another precision observation and a reanalysis of the 2012 data along with a reanalysis of a selection of three other objects from the literature (chosen using a strict set of restrictions to be able to argue for the desired accuracy) [40]. The resulting set of five absorbers yielded

$$\left(\frac{D}{H}\right)_p = (2.53 \pm 0.04) \times 10^{-5} \quad (8)$$

with a sample variance of only 0.05. We will use this value in our SBBN analysis below<sup>4</sup>.

---

<sup>4</sup> Note that the most recent measurement described in [81] has a somewhat larger uncertainty, and its

### C. Lithium

Lithium has by far the smallest observable primordial abundance in SBBN, but as we will see provides an important consistency check on the theory – a check that currently is not satisfied! In SBBN, mass-7 is made in the form of stable  ${}^7\text{Li}$ , but also as radioactive  ${}^7\text{Be}$ . In its neutral form,  ${}^7\text{Be}$  decays via electron capture with a half-life of 53 days. In the early universe, however, the decay is delayed until the universe is cool enough that  ${}^7\text{Be}$  can finally capture an electron at  $z \sim 30,000$  [82], shortly before hydrogen recombination! Thus  ${}^7\text{Be}$  decays long after the  $\sim 3$  min timescale of BBN, yet after recombination, all mass-7 takes the form of  ${}^7\text{Li}$ . Consequently,  ${}^7\text{Li}/\text{H}$  theory predictions sum both mass-7 isotopes. Note also that  ${}^7\text{Li}$  production dominates at low  $\eta$ , while  ${}^7\text{Be}$  dominates at high  $\eta$ , leading to the characteristic “lithium dip” versus baryon density in the Schramm plot (Fig. 1) described below.

A wide variety of astrophysical processes have been proposed as lithium nucleosynthesis sites operating after BBN. Cosmic-ray interactions with diffuse interstellar (or intergalactic) gas produces both  ${}^7\text{Li}$  and  ${}^6\text{Li}$  via spallation reaction such as  $p_{\text{cr}} + {}^{16}\text{O}_{\text{ism}} \rightarrow {}^{6,7}\text{Li} + \dots$ , and fusion  ${}^4\text{He}_{\text{cr}} + {}^4\text{He}_{\text{ism}} \rightarrow {}^{6,7}\text{Li} + \dots$  [83]. In the supernova “ $\nu$ -process,” neutrino spallation reactions can also produce  ${}^7\text{Li}$  in the helium shell via  $\nu + {}^4\text{He} \rightarrow {}^3\text{He}$  followed by  ${}^3\text{He} + {}^4\text{He} \rightarrow {}^7\text{Be} + \gamma$  as well as the mirror version of these [84] though the importance of this contribution to  ${}^7\text{Li}$  is limited by associated  ${}^{11}\text{B}$  production [85]. Finally, in somewhat lower mass stars undergoing the late, asymptotic giant branch phase of evolution,  ${}^3\text{He}$  burning leads to high surface Li abundances, some of that may (or may not!) survive to be ejected in the death of the stars [86]. Thus, despite its low abundance,  ${}^7\text{Li}$  is the only element with significant production in the Big Bang, stars, and cosmic rays; by contrast, the only conventional site of  ${}^6\text{Li}$  production is in cosmic ray interactions [70, 87].

To disentangle the diverse Li production processes observationally thus requires measurements of lithium abundances as a function of metallicity. As with  ${}^4\text{He}$ , the lowest-metallicity data should have negligible Galactic contribution and point to the primordial abundances. To date, the only systems for which such a metallicity evolution can be traced are in metal-poor (Population II) halo stars in our own Galaxy. As shown by Spite & Spite [88], halo main sequence (dwarf/subgiant) stars with temperatures  $T_{\text{eff}} \gtrsim 6000$  K have a constant Li

---

inclusion does not affect the weighted mean in Eq. (8)

abundance, while Li/H decreases markedly for cooler stars. The hotter stars have thin convection zones and so Li is not brought to regions hot enough to destroy it. These hot halo stars that seem to preserve their Li are thus of great cosmological interest. Spite & Spite [88] found that these stars with  $[\text{Fe}/\text{H}] \equiv \log[(\text{Fe}/\text{H})/(\text{Fe}/\text{H})_\odot] \lesssim -1.5$  have a substantially lower Li content than solar metallicity stars, and moreover the Li abundance does not vary with metallicity. This “Spite plateau” points to the primordial origin of Li. Furthermore, the Li/H abundance at the plateau gives the primordial value *if the host stars have not destroyed any of their lithium*.

The 1982 Spite plateau discovery was based on 11 stars in the plateau region. Since then, the number of stars on the plateau have increased by more than an order of magnitude. Increasingly precise observations showed that the scatter in Li abundances is very small for halo stars with metallicities down to  $[\text{Fe}/\text{H}] \sim -3$  [89–93].

Recently, thanks to huge increases in the numbers of known metal-poor halo stars, Li data has been extended to very low metallicity. Surprisingly, at metallicities below about  $[\text{Fe}/\text{H}] \lesssim -3$ , the Li/H scatter becomes large, in contrast to the small scatter in the Spite plateau found at slightly higher metallicity. In particular, the trend in extremely metal-poor stars is that no stars have Li/H above the Spite plateau value, a few are found near the plateau, but many lie significantly below [94, 95]. This “meltdown” of the Spite plateau remains difficult to understand from the point of view of stellar evolution, but in any case seems to demand that at least *some* halo stars have destroyed their Li. Moreover, as we will see below, this possibility has important consequences for the primordial lithium problem.

While the low-metallicity Li/H behavior is not understood, the Spite plateau remains at  $[\text{Fe}/\text{H}] \simeq -3$  to  $-1.5$ ; lacking a clear reason to discard these data, we will use them as a measure of primordial Li. Following ref. [94] we adopt their average of the non-meltdown halo stars having  $[\text{Fe}/\text{H}] \gtrsim -3$ , giving

$$\left(\frac{\text{Li}}{\text{H}}\right)_p = (1.6 \pm 0.3) \times 10^{-10}. \quad (9)$$

The stars in this sample were observed and analyzed in a uniform way, with Li abundances having been inferred from the absorption line spectra using sophisticated 3D stellar atmosphere models that do not assume local thermodynamic equilibrium (LTE).

Most halo star observations measure only elemental Li, because thermal broadening in the stellar atmospheres exceeds the isotope separation between  $^7\text{Li}$  and  $^6\text{Li}$ . However, very

high signal-to-noise measurements are sensitive to asymmetries in the  $\lambda 6707$  lineshape that encode this isotope information. There were recent claims of  ${}^6\text{Li}$  detections, with isotope ratios as high as  ${}^6\text{Li}/{}^7\text{Li} \lesssim 0.1$  [98]. The implied  ${}^6\text{Li}/\text{H}$  abundance lies far above the SBBN value, leading to a putative “ ${}^6\text{Li}$  problem.”

However, recent analyses with 3D, non-LTE stellar atmosphere models included surface convection effects (akin to solar granulation), and showed that these can entirely explain the observed line asymmetry [55, 56]. Thus case for  ${}^6\text{Li}$  detection in halo stars and for a  ${}^6\text{Li}$  problem, is weakened. Rather, the highest claimed  ${}^6\text{Li}/{}^7\text{Li}$  ratio is best interpreted as an upper limit.

#### D. The Cosmic Microwave Background

The cosmic microwave background (CMB) provides us with a snapshot of the universe at recombination ( $z_{\text{rec}} \simeq 1100$ ), and encodes a wealth of cosmological information at unprecedented precision. In particular, the CMB provides a particularly robust, precise measure of the cosmic baryon content, in a manner completely independent of BBN [6, 99–102]. Recently, the CMB determinations of  $N_{\text{eff}}$  and  $Y_p$  have also become quite interesting. In this section we will see how the precision of the CMB has changed the role of BBN in cosmology, and enhanced the leverage of BBN to probe new physics.

The physics of the CMB, and its relation to cosmological parameters, is recounted in excellent reviews such as [103]. Here, we briefly and qualitatively summarize some of the key physics of the recombination epoch ( $z_{\text{rec}} \simeq 1100$ ) when the CMB was released.

Tiny primordial density fluctuations are laid down in the very early universe, by inflation or some other mechanism. After matter-radiation equality,  $z_{\text{eq}} \simeq 3400$ , the dark matter density fluctuations grow and form increasingly deep gravitational potentials. The baryon-electron plasma is attracted to the potential wells, and undergoes adiabatic compression as it falls in. Prior to recombination, the plasma remains tightly coupled to the CMB photons, whose pressure  $P_\gamma \propto T^4$  acting as a restoring force, with sound speed  $c_s^2 \sim 1/3$ . This interplay of forces leads to acoustic oscillations of the plasma. The oscillations continue until (re)combination, when the universe goes from an opaque plasma to a transparent gas of neutral H and He. The decoupled photons for the most part travel freely thereafter until detection today, recording a snapshot of the recombining universe.



Because the density fluctuations are small, perturbations in the cosmic fluids are very well described by linear theory, wherein different wavenumbers evolve independently. Modes that have just attained their first contraction to a density maximum at recombination occur at the sound horizon  $\sim c_s t_{\text{rec}}$ . This lengthscale projects onto the sky to a characteristic angular scale  $\sim 1^\circ$ ; this corresponds to the first and strongest peak in the CMB angular power spectrum. Higher harmonics correspond to modes at other density extrema. The acoustic oscillations depend on the cosmology as well as the plasma properties, which set the angular scales of the harmonics as well as the heights of the features, as well as the correspondence between the temperature anisotropies and the polarization. This gives rise to the CMB sensitivity to cosmological parameters.

Precision observations of CMB temperature and polarization fluctuations over a wide range of scales now exist, and probe a host of cosmological parameters. Fortunately for BBN, one of the most robust of these is the cosmic baryon content, usually quantified in the CMB literature via the plasma (baryon + electron) density  $\rho_b$  written as the density parameter  $\Omega_b \equiv \rho_b/\rho_{\text{crit}}$  where the critical density  $\rho_{\text{crit}} = 3H_0^2/8\pi G$ , with  $H_0 = 100 h \text{ km s}^{-1} \text{ Mpc}^{-1}$  the present Hubble parameter. This in turn is related to the baryon-to-photon ratio  $\eta$  via

$$\eta = \frac{\rho_{\text{crit}}}{\langle m \rangle n_\gamma^0} \Omega_B, \quad (10)$$

where  $n_\gamma^0 = 2\zeta(3)T_0^3/\pi^2$  is the present-day photon number density. The mean mass per baryon  $\langle m \rangle$  in eq. (10) is roughly the proton mass, but slightly lower due to the binding energy of helium. As a result, the detailed conversion depends very mildly on the  $^4\text{He}$  abundance [104], and we have

$$\eta_{10} = 273.3036 \Omega_B h^2 \left(1 + 7.16958 \times 10^{-3} Y_p\right) \left(\frac{2.7255 K}{T_\gamma^0}\right)^3. \quad (11)$$

The CMB also encodes the values of  $Y_p$  and  $N_{\text{eff}}$  at recombination. The effect of helium and thus  $Y_p$  is to set the number of plasma electrons per baryon. This controls the Thomson scattering mean free path  $(\sigma_T n_e)^{-1}$  that sets the scale at which the acoustic peaks are damped (exponentially!) by photon diffusion. The effect of radiation and thus of  $N_{\text{eff}}$  is predominantly to increase the cosmic expansion rate via  $H^2 \propto \rho$ . This also affects the scale of damping onset, when the diffusion length is comparable to the sound horizon [105]. Thus, measurements of the CMB damping tail at small angular scales (high  $\ell$ ) probe both  $Y_p$  and  $N_{\text{eff}}$ . In fact, the CMB determinations of these quantities are strongly anticorrelated—a

higher  $Y_p$  implies a lower diffusion mean free path, which is equivalent to a larger sound horizon  $\sim \int da/aH$  and thus lower  $N_{\text{eff}}$ .

Since the first *WMAP* results in 2003 [99] sharply measured the first acoustic peaks, the CMB has determined  $\eta$  more precisely than BBN. Moreover, both ground-based and *Planck* data now measure the damping tail with sufficient accuracy to simultaneously probe all of  $(\Omega_b h^2, Y_p, N_{\text{eff}})$  [6, 106, 107]. Of course, BBN demands an essentially unique relationship among these quantities. *Thus, it is now possible to meaningfully test BBN and thus cosmology via CMB measurements alone!*

We adopt CMB determinations of  $(\Omega_b h^2, Y_p, N_{\text{eff}})$  from *Planck* 2015 data, as described in detail below, §IV C. We note in passing that these CMB constraints rely on the present CMB temperature,  $T_\gamma^0$ , which is held fixed in the *Planck* analysis we use. In the future,  $T_\gamma^0$  should be varied in the CMB data evaluation, in order to provide the most stringent constraint on the relative number of baryons in the universe.

#### IV. THE LIKELIHOOD ANALYSIS

As data analysis improved, theoretical studies of BBN moved toward a more rigorous approach using Monte-Carlo techniques in likelihood analyses [108–111]. Thus, in order to make quantitative statements about the light element predictions and convolutions with CMB constraints, we need probability distributions for our BBN predictions, for the light element observations and CMB-constrained parameters. We discuss here how we propagate nuclear reaction rate uncertainties into the BBN light element abundance predictions, how we determine the CMB-parameter likelihood distributions, and how we combine them to make stronger constraints.

##### A. Monte-Carlo Predictions for the Light Elements

The dominant source of uncertainty in the BBN light-element predictions stem from experimental uncertainties of nuclear reaction rates. We propagate these uncertainties by randomly drawing rates according their adopted probability distributions for each BBN evaluation. We choose a Monte Carlo of size  $N = 10000$ , keeping the error in the mean and error in the error at the 1% level. It is important that we use the same random numbers

for each set of parameters  $(\eta, N_\nu)$ . This helps remove any extra noise from the Monte Carlo predictions and allows for smooth interpolations between parameter points.

For each grid point of parameter values we calculate the means and covariances of the light element abundance predictions. We add the  $1/\sqrt{N}$  errors in quadrature to our evaluated uncertainties on the light element predictions. We have examined the light element abundance distributions, by calculating higher order statistics (skewness and kurtosis), and by histogramming the resultant Monte Carlo points and verified that they are well-approximated with log-normal or gaussian distributions.

In standard BBN, the baryon-to-photon ratio ( $\eta$ ) is the only free parameter of the theory. Our Monte Carlo error propagation is summarized in Figure 1, which plots the light element abundances as a function of the baryon density (upper scale) and  $\eta$  (lower scale). The abundance for He is shown as the mass fraction  $Y$ , while the abundances of the remaining isotopes of D,  $^3\text{He}$ , and  $^7\text{Li}$  are shown as abundances by number relative to H. The thickness of the curves show the  $\pm 1\sigma$  spread in the predicted abundances. These results assume  $N_\nu = 3$  and the current measurement of the neutron lifetime  $\tau_n = 880.3 \pm 1.1$  s.

Using a Monte Carlo approach also allows us to extract sensitivities of the light element predictions to reaction rates and other parameters. The sensitivities are defined as the logarithmic derivatives of the light element abundances with respect to each variation about our fiducial model parameters [112], yielding a simple relation for extrapolating about the fiducial model:

$$X_i = X_{i,0} \prod_n \left( \frac{p_n}{p_{n,0}} \right)^{\alpha_n}, \quad (12)$$

where  $X_i$  represents either the helium mass fraction or the abundances of the other light elements by number. The  $p_n$  represent input quantities to the BBN calculations ( $\eta, N_\nu, \tau_n$ ) and the gravitational constant  $G_N$  as well key nuclear rates which affect the abundance  $X_i$ .  $p_{n,0}$  refers to our standard input value. The information contained in Eqs. (13-17) are neatly summarized in Table III.

$$Y_p = 0.24703 \left( \frac{10^{10}\eta}{6.10} \right)^{0.039} \left( \frac{N_\nu}{3.0} \right)^{0.163} \left( \frac{G_N}{G_{N,0}} \right)^{0.35} \left( \frac{\tau_n}{880.3s} \right)^{0.73} \\ \times [p(n, \gamma)d]^{0.005} [d(d, n)^3\text{He}]^{0.006} [d(d, p)t]^{0.005} \quad (13)$$

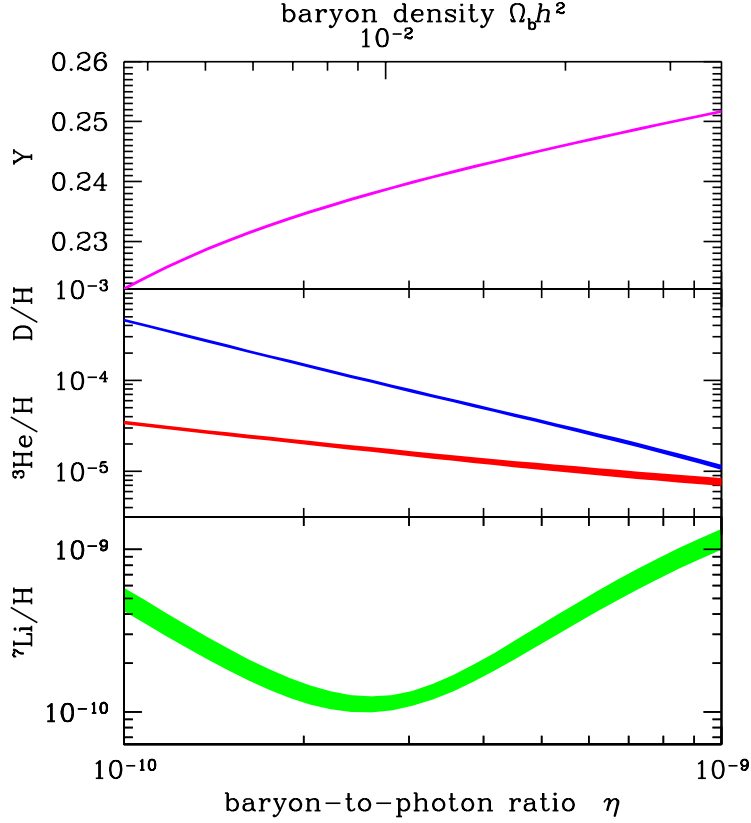


FIG. 1. Primordial abundances of the light nuclides as a function of cosmic baryon content, as predicted by SBBN (“Schramm plot”). These results assume  $N_\nu = 3$  and the current measurement of the neutron lifetime  $\tau_n = 880.3 \pm 1.1$  s. Curve widths show  $1 - \sigma$  errors.

$$\begin{aligned} \frac{D}{H} &= 2.579 \times 10^{-5} \left( \frac{10^{10} \eta}{6.10} \right)^{-1.60} \left( \frac{N_\nu}{3.0} \right)^{0.395} \left( \frac{G_N}{G_{N,0}} \right)^{0.95} \left( \frac{\tau_n}{880.3s} \right)^{0.41} \\ &\times [p(n, \gamma)d]^{-0.19} [d(d, n)^3\text{He}]^{-0.53} [d(d, p)t]^{-0.47} \\ &\times [d(p, \gamma)^3\text{He}]^{-0.31} [^3\text{He}(n, p)t]^{0.023} [^3\text{He}(d, p)^4\text{He}]^{-0.012} \end{aligned} \quad (14)$$

$$\begin{aligned} \frac{^3\text{He}}{H} &= 9.996 \times 10^{-6} \left( \frac{10^{10} \eta}{6.10} \right)^{-0.59} \left( \frac{N_\nu}{3.0} \right)^{0.14} \left( \frac{G_N}{G_{N,0}} \right)^{0.34} \left( \frac{\tau_n}{880.3s} \right)^{0.15} \\ &\times [p(n, \gamma)d]^{0.088} [d(d, n)^3\text{He}]^{0.21} [d(d, p)t]^{-0.27} \\ &\times [d(p, \gamma)^3\text{He}]^{0.38} [^3\text{He}(n, p)t]^{-0.17} [^3\text{He}(d, p)^4\text{He}]^{-0.76} [t(d, n)^4\text{He}]^{-0.009} \end{aligned} \quad (15)$$

$$\frac{^7\text{Li}}{H} = 4.648 \times 10^{-10} \left( \frac{10^{10} \eta}{6.10} \right)^{2.11} \left( \frac{N_\nu}{3.0} \right)^{-0.284} \left( \frac{G_N}{G_{N,0}} \right)^{-0.73} \left( \frac{\tau_n}{880.3s} \right)^{0.43}$$

$$\begin{aligned}
& \times [p(n, \gamma)d]^{1.34} [d(d, n)^3\text{He}]^{0.70} [d(d, p)t]^{0.065} \\
& \times [d(p, \gamma)^3\text{He}]^{0.59} [^3\text{He}(n, p)t]^{-0.27} [^3\text{He}(d, p)^4\text{He}]^{-0.75} [t(d, n)^4\text{He}]^{-0.023} \\
& \times [^3\text{He}(\alpha, \gamma)^7\text{Be}]^{0.96} [^7\text{Be}(n, p)^7\text{Li}]^{-0.71} [^7\text{Li}(p, \alpha)^4\text{He}]^{-0.056} [t(\alpha, \gamma)^7\text{Li}]^{0.030} \quad (16)
\end{aligned}$$

$$\begin{aligned}
\frac{^6\text{Li}}{\text{H}} &= 1.288 \times 10^{-13} \left( \frac{10^{10}\eta}{6.10} \right)^{-1.51} \left( \frac{N_\nu}{3.0} \right)^{0.60} \left( \frac{G_N}{G_{N,0}} \right)^{1.40} \left( \frac{\tau_n}{880.3s} \right)^{1.37} \\
& \times [p(n, \gamma)d]^{-0.19} [d(d, n)^3\text{He}]^{-0.52} [d(d, p)t]^{-0.46} \\
& \times [d(p, \gamma)^3\text{He}]^{-0.31} [^3\text{He}(n, p)t]^{0.023} [^3\text{He}(d, p)^4\text{He}]^{-0.012} [d(\alpha, \gamma)^6\text{Li}]^{1.00} \quad (17)
\end{aligned}$$

TABLE III. This table contains the sensitivities,  $\alpha_n$ 's defined in Eq. 12 for each of the light element abundance predictions, varied with respect to key parameters and reaction rates.

Variant	$Y_p$	D/H	$^3\text{He}/\text{H}$	$^7\text{Li}/\text{H}$	$^6\text{Li}/\text{H}$
$\eta$ ( $6.1 \times 10^{-10}$ )	0.039	-1.598	-0.585	2.113	-1.512
$N_\nu$ (3.0)	0.163	0.395	0.140	-0.284	0.603
$G_N$	0.354	0.948	0.335	-0.727	1.400
n-decay	0.729	0.409	0.145	0.429	1.372
p(n, $\gamma$ )d	0.005	-0.194	0.088	1.339	-0.189
$^3\text{He}(n,p)t$	0.000	0.023	-0.170	-0.267	0.023
$^7\text{Be}(n,p)^7\text{Li}$	0.000	0.000	0.000	-0.705	0.000
d(p, $\gamma$ ) $^3\text{He}$	0.000	-0.312	0.375	0.589	-0.311
d(d, $\gamma$ ) $^4\text{He}$	0.000	0.000	0.000	0.000	0.000
$^7\text{Li}(p,\alpha)^4\text{He}$	0.000	0.000	0.000	-0.056	0.000
d( $\alpha, \gamma$ ) $^6\text{Li}$	0.000	0.000	0.000	0.000	1.000
t( $\alpha, \gamma$ ) $^7\text{Li}$	0.000	0.000	0.000	0.030	0.000
$^3\text{He}(\alpha, \gamma)^7\text{Be}$	0.000	0.000	0.000	0.963	0.000
d(d,n) $^3\text{He}$	0.006	-0.529	0.213	0.698	-0.522
d(d,p)t	0.005	-0.470	-0.265	0.065	-0.462
t(d,n) $^4\text{He}$	0.000	0.000	-0.009	-0.023	0.000
$^3\text{He}(d,p)^4\text{He}$	0.000	-0.012	-0.762	-0.752	-0.012

## B. The Neutron Mean Life

As noted in the introduction, the value of the neutron mean life has had a turbulent history. Unfortunately, the predictions of SBBN remain sensitive to this quantity. This sensitivity is displayed in the scatter plot of our Monte Carlo error propagation with fixed  $\eta = 6.10 \times 10^{-10}$  in Figure 2. The correlation between the neutron mean lifetime and  $^4\text{He}$  abundance prediction is clear. The correlation is not infinitesimally narrow because other reaction rate uncertainties significantly contribute to the total uncertainty in  $^4\text{He}$ .

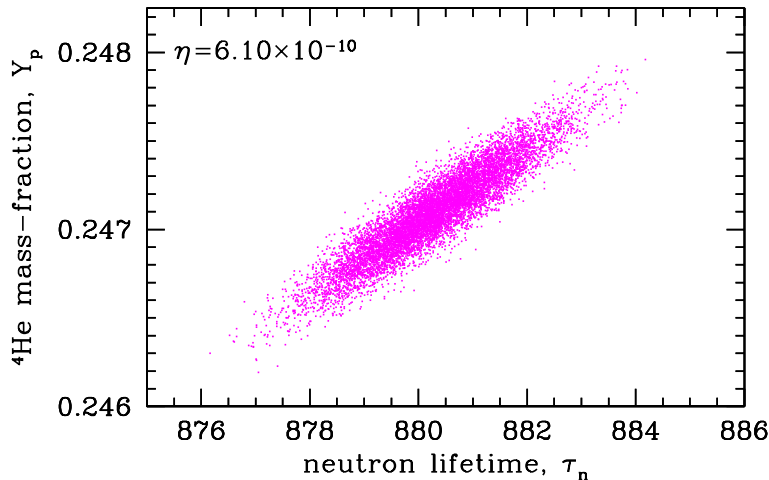


FIG. 2. The sensitivity of the  $^4\text{He}$  abundance to the neutron mean life, as shown through a scatter plot of our Monte Carlo error propagation.

## C. *Planck* Likelihood Functions

For this paper, we will need to consider two sets of *Planck* Markov Chain data, one for standard BBN (SBBN) and one for non-standard BBN (NBBN). Using the *Planck* Markov chain data [113], we have constructed the multi-dimensional likelihoods for the following extended parameter chains, **base\_yhe** and **base\_nnu\_yhe**, for the `plikHM.TTTEEE.lowTEB` dataset. As noted earlier, we do not use the *Planck* base chain, as it assumes a BBN relationship between the helium abundance and the baryon density.

From these 2 parameter sets we have the following 2- and 3-dimensional likelihoods

from the CMB:  $\mathcal{L}_{\text{PLA}+\text{base\_yhe}}(\omega_b, Y_p)$  and  $\mathcal{L}_{\text{PLA}+\text{base\_nnu\_yhe}}(\omega_b, Y_p, N_\nu)$ . The 2-dimensional **base\_yhe** likelihood is well-represented by a 2D correlated gaussian distribution, with means and standard deviations for the baryon density and  $^4\text{He}$  mass fraction

$$\omega_b = 0.022305 \pm 0.000225 \quad (18)$$

$$Y_p = 0.25003 \pm 0.01367 \quad (19)$$

and a correlation coefficient  $r \equiv \text{cov}(\omega_b, Y_p) / \sqrt{\text{var}(\omega_b)\text{var}(Y_p)} = +0.7200$ .

The two parameter data can be marginalized to yield 1-dimensional likelihood functions for  $\eta$ . The peak and  $1-\sigma$  spread in  $\eta$  is given in the first row of Table IV. The following rows correspond to different determinations of  $\eta$ . In the second-fourth rows, no CMB data is used. That is, we fix  $\eta$  only from the observed abundances of  $^4\text{He}$ , D or both. Notice for example, in row 2, the value for  $\eta$  is low and has a huge uncertainty. This is due to the slightly low value for the observational abundance (7) and the logarithmic dependence of  $Y_p$  on  $\eta$ . We see again that BBN+ $Y_p$  is a poor baryometer. This will be described in more detail in the following subsection. Row 5, uses the BBN relation between  $\eta$  and  $Y_p$ , but no observational input from  $Y_p$  is used. This is closest to the *Planck* determination found in [6], though here  $Y_p$  was taken to be free and the value of  $\eta$  in the Table is a result of marginalization over  $Y_p$ . This accounts for the very small difference in the results for  $\eta$ :  $\eta_{10} = 6.09$  (*Planck*);  $\eta_{10} = 6.10$  (Table IV). Rows 6-8 add the observational determinations of  $^4\text{He}$ , D and the combination. As one can see, the inclusion of the observational data does very little to affect the determination of  $\eta$  and thus we use  $\eta_{10} = 6.10$  as our fiducial baryon-to-photon ratio.

The 3-dimensional **base\_nnu\_yhe** likelihood is *not* well-represented by a simple 3D correlated gaussian distribution, but since these distributions are single-peaked we can correct for the non-gaussianity via a 3D Hermite expansion about a 3D correlated gaussian base distribution. Details of this prescription will be given in the Appendix.

The calculated mean values and standard deviations for these distributions are:

$$\omega_b = 0.022212 \pm 0.000242 \quad (20)$$

$$N_{\text{eff}} = 2.7542 \pm 0.3064 \quad (21)$$

$$Y_p = 0.26116 \pm 0.01812 \quad (22)$$

These values correspond to the peak of the likelihood distribution using CMB data alone. That is, no use is made of the correlation between the baryon density and the helium

TABLE IV. Constraints on the baryon-to-photon ratio, using different combinations of observational constraints. We have marginalized over  $Y_p$  to create 1D  $\eta$  likelihood distributions.

Constraints Used	$\eta \times 10^{10}$
CMB-only	$6.108 \pm 0.060$
BBN+ $Y_p$	$4.87^{+2.46}_{-1.54}$
BBN+D	$6.180 \pm 0.195$
BBN+ $Y_p$ +D	$6.172 \pm 0.195$
CMB+BBN	$6.098 \pm 0.042$
CMB+BBN+ $Y_p$	$6.098 \pm 0.042$
CMB+BBN+D	$6.102 \pm 0.041$
CMB+BBN+ $Y_p$ +D	$6.101 \pm 0.041$

abundance through BBN. For this reason, the helium mass fraction is found to be rather high. Our value of  $Y_p = 0.261 \pm 0.36(2\sigma)$  can be compared with the value given by the *Planck* collaboration [6] of  $Y_p = 0.263^{+0.34}_{-0.37}$ .

In this case, we marginalize to form a 2-d likelihood function to determine both  $\eta$  and  $N_{\text{eff}}$ . As in the 1-d case discussed above, we can determine  $\eta$  and  $N_\nu$  using CMB data alone. This result is shown in row 1 of Table V and does not use any correlation between  $\eta$  and  $Y_p$ . Note that the value of  $N_\nu$  given here differs from that in Eq. (21) since the value in the Table comes from a marginalized likelihood function, where as the value in the equation does not. Row 2, uses only BBN and the observed abundances of  $^4\text{He}$  and D with no direct information from the CMB. Rows 3-6 use the combination of the CMB data, together with the BBN relation between  $\eta$  and  $Y_p$  with and without the observational abundances as denoted. As one can see, opening up the parameter space to allow  $N_\nu$  to float induces a relatively small drop  $\eta$  (by a fraction of 1  $\sigma$ ) and the peak for  $N_\nu$  is below the Standard Model value of 3 though consistent with that value within 1  $\sigma$ .

We note that we have been careful to use the appropriate relation between  $\eta$  and  $\omega_b$  via Eq. 11. Also, in our NBBN calculations we formally use the number of neutrinos, *not* the *effective* number of neutrinos, thus demanding the relation:  $N_{\text{eff}} = 1.015333N_\nu$ . For the 2D **base\_yhe** CMB likelihoods, we include the higher order skewness and kurtosis terms to more accurately reproduce the tails of the distributions.



TABLE V. The marginalized most-likely values and central 68.3% confidence limits on the baryon-to-photon ratio and effective number of neutrinos, using different combinations of observational constraints.

Constraints Used	$\eta_{10}$	$N_\nu$
CMB-only	$6.08 \pm 0.07$	$2.67^{+0.30}_{-0.27}$
BBN+ $Y_p$ +D	$6.10 \pm 0.23$	$2.85 \pm 0.28$
CMB+BBN	$6.08 \pm 0.07$	$2.91 \pm 0.20$
CMB+BBN+ $Y_p$	$6.07 \pm 0.06$	$2.89 \pm 0.16$
CMB+BBN+D	$6.07 \pm 0.07$	$2.90 \pm 0.19$
CMB+BBN+ $Y_p$ +D	$6.07 \pm 0.06$	$2.88 \pm 0.16$

#### D. Results: The Likelihood Functions

Applying the formalism described above, we derive the likelihood functions for SBBN and NBBN that are our central results. Turning first to SBBN, we fix  $N_\nu = 3$  and use the *Planck* determination of  $\eta$  as the sole *input* to BBN in order to derive CMB+BBN predictions for each light element. That is, for each light element species  $X_i$  we evaluate the likelihood

$$\mathcal{L}(X_i) \propto \int \mathcal{L}_{\text{PLA-base-ye}}(\omega_b, Y_p) \mathcal{L}_{\text{BBN}}(\eta; \{X_i\}) d\eta \quad (23)$$

where  $\mathcal{L}_{\text{BBN}}(\eta; \{X_i\})$  comes from our BBN Monte Carlo, and where we use the  $\eta - \omega_b$  relation in eq. (11). In the case of  $^4\text{He}$ , we use only the CMB  $\eta$  to determine the  $X_i = Y_{p,\text{BBN}}$  prediction and compare this to the CMB-only prediction.

The resulting CMB+BBN abundance likelihoods appear as the dark-shaded (purple, solid line) curves in Figure 3, which also shows the observational abundance constraints (§III) in the light-shaded (yellow, dashed-line) curves. In panel (a), we see that the  $^4\text{He}$  BBN+CMB likelihood is markedly more narrow than its observational counterpart, but the two are in near-perfect agreement. The medium-shaded (cyan, dotted line) curve in this panel is the CMB-only  $Y_p$  prediction, which is the least precise but also completely consistent with the other distributions. Panel (b) displays the dramatic consistency between the CMB+BBN deuterium prediction and the observed high- $z$  abundance. Moreover, we see that the D/H observations are substantially more precise than the theory. Panel (c) shows the primordial  $^3\text{He}$  prediction, for which there is no reliable observational test at present. Finally, panel

(d) reveals a sharp discord between the BBN+CMB prediction for  ${}^7\text{Li}$  and the observed primordial abundance—the two likelihoods are essentially disjoint.

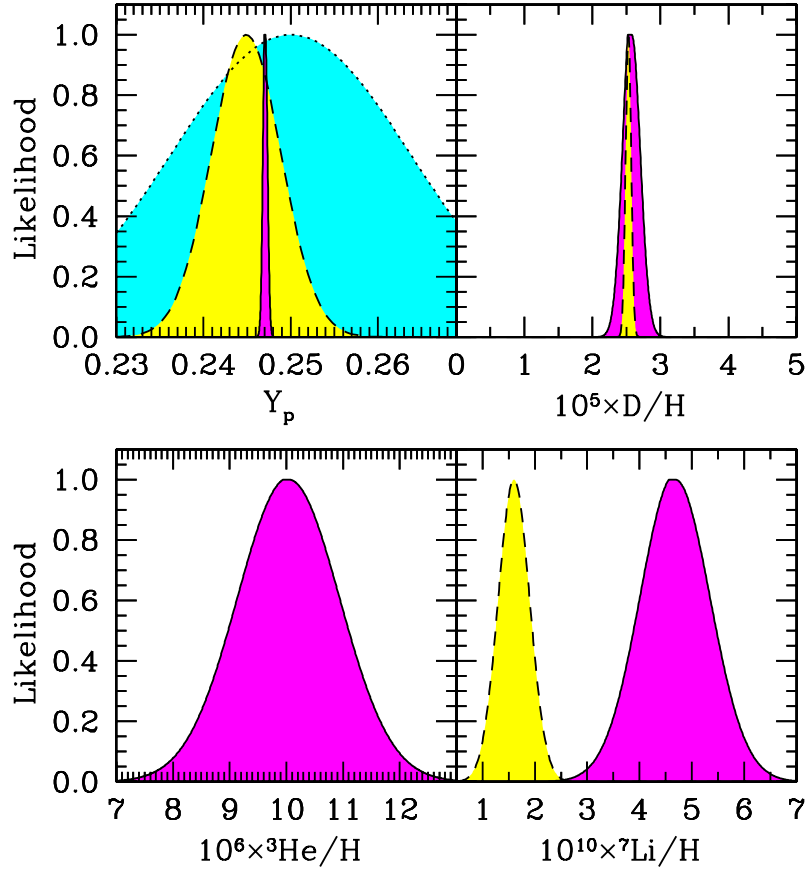


FIG. 3. Light element predictions using the CMB determination of the cosmic baryon density. Shown are likelihoods for each of the light nuclides, normalized to show a maximum value of 1. The solid-lined, dark-shaded (purple) curves are the BBN+CMB predictions, based on *Planck* inputs as discussed in the text. The dashed-lined, light-shaded (yellow) curves show astronomical measurements of the primordial abundances, for all but  ${}^3\text{He}$  where reliable primordial abundance measures do not exist. For  ${}^4\text{He}$ , the dotted-lined, medium-shaded (cyan) curve shows the CMB determination of  ${}^4\text{He}$ .

Figure 3 represents not only a quantitative assessment of the concordance of BBN, but also a test of the standard big bang cosmology. If we limit our attention to each element

in turn, we are struck by the spectacular agreement between D/H observations at  $z \sim 3$  and the BBN+CMB predictions combining physics at  $z \sim 10^{10}$  and  $z \sim 1000$ . The consistency among all three  $Y_p$  determinations is similarly remarkable, and the joint concordance between D and  ${}^4\text{He}$  represents a non-trivial success of the hot big bang model. Yet this concordance is not complete: the pronounced discrepancy in  ${}^7\text{Li}$  measures represents the “lithium problem” discussed below (§V). This casts a shadow of doubt over SBBN itself, pending a firm resolution of the lithium problem, and until then the BBN/CMB concordance remains an incomplete success for cosmology.

Quantitatively, the likelihoods in Fig. 3 are summarized by the predicted abundances

$$Y_p = 0.24709 \pm 0.00025 \quad (24)$$

$$\text{D/H} = (2.58 \pm 0.13) \times 10^{-5} \quad (25)$$

$${}^3\text{He/H} = (10.039 \pm 0.090) \times 10^{-5} \quad (26)$$

$${}^7\text{Li/H} = (4.68 \pm 0.67) \times 10^{-10} \quad (27)$$

$$\log_{10}({}^6\text{Li/H}) = -13.89 \pm 0.20 \quad (28)$$

where the central value give the mean, and the error the  $1\sigma$  variance. The slightly differences from the values in Table II arise due to the Monte Carlo averaging procedure here as opposed to evaluating the abundance using central values of all inputs at a single  $\eta$ .

We see that the BBN/CMB comparison is enriched now that the CMB has achieved an interesting sensitivity to  $Y_p$  as well as  $\eta$ . This interplay is further illustrated in Figure 4, which shows 2-D likelihood contours in the  $(\eta, Y_p)$  plane, still for fixed  $N_\nu = 3$ . The *Planck* contours show a positive correlation between the CMB-determined baryon density and helium abundance. Also plotted is the BBN relation for  $Y_p(\eta)$ , which for SBBN is a *zero-parameter curve* that is very tight even including its small width due to nuclear reaction rate uncertainties. We see that the curve goes through the heart of the CMB predictions, which represents a novel and non-trivial test of SBBN *based entirely on CMB data* without any astrophysical input. This agreement stands as a triumph for SBBN and the hot big bang, and illustrates the still-growing power of the CMB as a cosmological probe.

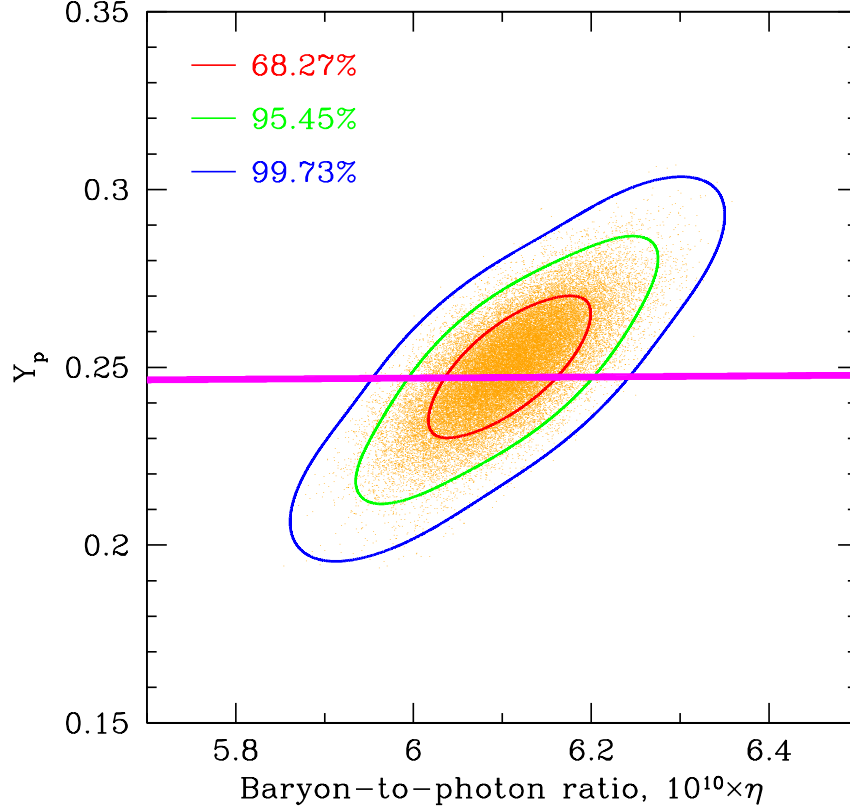


FIG. 4. The 2D likelihood function contours derived from the *Planck* Markov Chain Monte Carlo **base\_yhe** [113] with fixed  $N_\nu = 3$  (points). The correlation between  $Y_p$  and  $\eta$  is evident. The  $3\text{-}\sigma$  BBN prediction for the helium mass fraction is shown with the colored band. We see that including the BBN  $Y_p(\eta)$  relation significantly reduces the uncertainty in  $\eta$  due to the CMB  $Y_p - \eta$  correlation.

Thus far we have used the CMB  $\eta$  as an input to BBN; we conclude this section by studying the constraints on  $\eta$  when jointly using BBN theory, light-element abundances, and the CMB in various combinations. Figure 5 shows the  $\eta$  likelihoods that result from a set of such combinations. Setting aside at first the CMB, the BBN+ $X$  curves show the combination of BBN theory and astrophysical abundance observations,  $\mathcal{L}_{\text{BBN}+X}(\eta) = \int \mathcal{L}_{\text{BBN}}(\eta, X) \mathcal{L}_{\text{obs}}(X) dX$ , with  $X \in (Y_p, \text{D/H})$ . The CMB-only curve marginalizes over the *Planck*  $Y_p$  values  $\mathcal{L}_{\text{CMB-only}}(\eta) = \int \mathcal{L}_{\text{PLA-base\_yhe}}(\omega_b, Y_p) dY_p$  where we use the  $\eta - \omega_b$  relation in eq. (11). The BBN+CMB curve adds the BBN  $Y_p(\eta)$  relation. Finally, BBN+CMB+D

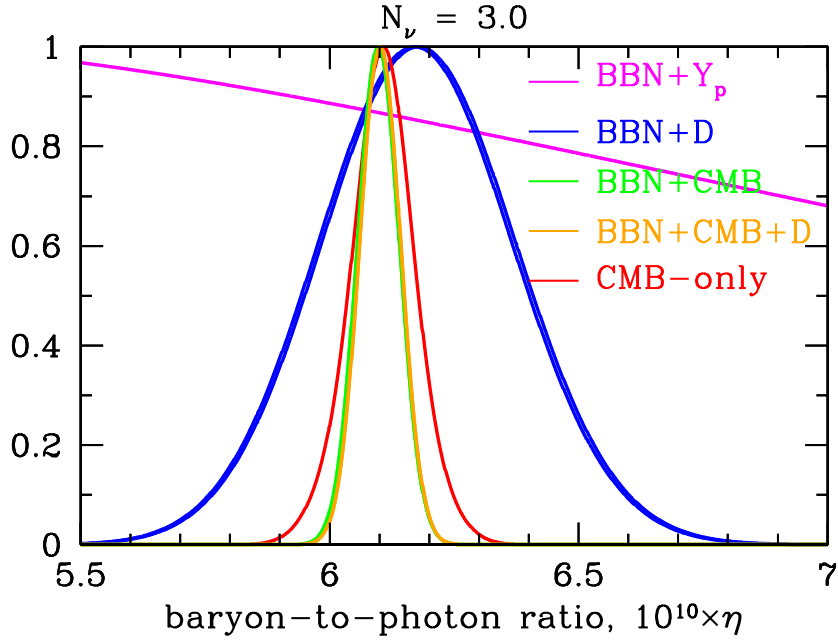


FIG. 5. The likelihood distributions of the baryon-to-photon ratio parameter,  $\eta$ , given various CMB and light-element abundance constraints.

also includes the observed primordial deuterium.

We see in Fig. 5 that of the primordial abundance observations, deuterium is the only useful “baryometer,” due to its strong dependence on  $\eta$  in the Schramm plot (Fig. 1). By contrast,  $^4\text{He}$  alone offers no useful constraint on  $\eta$ , tracing back to the weak  $Y_p(\eta)$  trend in Fig. 1. The CMB alone has now surpassed BBN+D in measuring the cosmic baryon content, but an even stronger limit comes from BBN+CMB. As seen in Fig. 4, this tightens the  $\eta$  constraint due to the CMB correlation between  $Y_p$  and  $\eta$ . Finally BBN+CMB+D provides only negligibly stronger limits. The peaks of the likelihoods correspond to the values in

Table IV, and the tightest constraints are all consistent with our adopted central value  $\eta = 6.10 \times 10^{-10}$ .

## V. THE LITHIUM PROBLEM

As seen in the panels of Fig. 3 above, the observed primordial lithium abundance differs sharply from the BBN+CMB prediction [19]. This discrepancy constitutes the “Lithium Problem”, which was foreshadowed before CMB determinations of  $\eta$ , and has persisted over the dozen years since the first *WMAP* data release. For a detailed recent review of the lithium problem, see [114]. Here we briefly summarize the current status.

The most conventional means to resolve the primordial lithium problem invokes large lithium depletion in halo stars [46]. As noted above (§III C), recent observations of the Spite plateau “meltdown” at very low metallicity,  $[\text{Fe}/\text{H}] < -3$ , seem to demand that *some* stars have depleted their lithium [94, 95]. Could the other plateau halo stars have also destroyed their lithium? Such a scenario cannot be ruled out, but raises other questions that remain unanswered: why is the Li/H dispersion so small at metallicities above the “meltdown”? And why is there a “lithium desert” with no stars having lithium abundances between the plateau and the primordial abundance?

It is worthwhile to find other sites for Li/H measurements, as clearly halo star lithium depletion is theoretically complex and observationally challenging. Unfortunately, the CMB itself does not yet provide an observable signature of primordial lithium [96]. However, a promising new direction is the observation of interstellar lithium in low-metallicity or high- $z$  galaxies [97]. Interstellar measurements in the Small Magellanic Cloud (metallicity  $\sim 1/4$  solar) find  $\text{Li}/\text{H}_{\text{ISM,SMC}} = (4.8 \pm 1.8) \times 10^{-10}$  [115]. This value is consistent with the CMB+BBN primordial abundance, but the SMC is far from primordial, with a metallicity of about  $1/4$  solar. Indeed, the SMC interstellar lithium abundance *agrees* with that of Milky Way stars at the same  $[\text{Fe}/\text{H}]$ , which are disk (Population I) stars in which Li/H is rising from the Spite plateau due to Galactic production. Thus we see consistency between lithium abundances at the same metallicity, but measured in very different systems with very different systematics. This strongly suggests that stellar lithium depletion has not been underestimated, at least down to this metallicity. Moreover, this observation serves as a proof-of-concept demonstration that measurements of interstellar lithium in galaxies with

lower metallicities would could strongly test stellar depletion and potentially rule out this solution to the lithium problem.

Another means of resolving the lithium problem within the context of the standard cosmology and Standard Model microphysics is to alter the BBN theory predictions due to revisions in nuclear reaction rates [17, 41, 42]. But as we have seen, all of the reactions that are ordinarily the most important for BBN have been well measured at the energies of interest. Typically, cross sections are known to  $\sim 10\%$  or better, and these errors are already folded into Fig. 3. A remaining possibility is that a reaction thought to be unimportant could contain a *resonance* heretofore unknown, which could boost its cross section enormously, analogously to the celebrated Hoyle  $^{12}\text{C}$  resonance that dominates the  $3\alpha \rightarrow ^{12}\text{C}$  rate [116].

In BBN, the densities and timescales prior to nuclear freezeout are such that only two-body reactions are important, and it is possible to systematically study all two-body reactions that enhance the destruction of  $^7\text{Be}$ . A small number candidates emerge, for which one can make definite predictions of the needed resonant state energy and width:  $^7\text{Be}(d, \gamma)^9\text{B}$ ,  $^7\text{Be}(^3\text{He}, \gamma)^{10}\text{C}$ , and  $^7\text{Be}(t, \gamma)^{10}\text{B}$  [43–45]. However, measurements in  $^7\text{Be}(d, d)^7\text{Be}$  [117],  $^9\text{Be}(^3\text{He}, t)^9\text{B}$  [118], and an *R*-matrix analysis of  $^9\text{B}$  [119] all rule out a  $^9\text{B}$  resonance. Similarly,  $^{10}\text{C}$  data rule out the needed resonance in  $^{10}\text{C}$  [120]. The upshot is that a “nuclear option” to the lithium problem is essentially excluded.

It is thus a real possibility that the lithium problem may point to new physics at play during or after nucleosynthesis. A number of possible solutions have been proposed and are discussed in the reviews cited above. Here we simply note that a challenge to all such models is that they must reduce  $^7\text{Li}$  substantially, yet *not* perturb the other light elements unacceptably. Generally, there is a tradeoff between  $^7\text{Be}$  destruction and D production (usually as a by-product of  $^4\text{He}$  disruption) [76, 121]. Essentially all successful models drive D/H to the maximum abundance allowed by observations. However, the new very precise D/H measurements (§III B) dramatically reduce the allowed perturbations and will challenge most of the existing new-physics solutions to the lithium problem. It remains to be seen whether it is possible to introduce new physically-motivated perturbations that satisfy the D/H constraint while still solving or at least substantially reducing the lithium problem.

## VI. LIMITS ON $N_{\text{eff}}$

Before concluding, we consider a one-parameter extension of SBBN by allowing the number of relativistic degrees of freedom to differ from the Standard Model value of  $N_\nu = 3$  and  $N_{\text{eff}} = 3.046$ . Opening this degree of freedom has an impact on both the CMB and BBN. In Fig. 6, the thinner contours show the 2D likelihood distribution in the  $(\eta, N_\nu)$  plane, using *Planck* data marginalizing over the CMB  $Y_p$ . We see that the CMB  $N_\nu$  values are nearly uncorrelated with  $\eta$ . The thicker contours include BBN information and are discussed below.

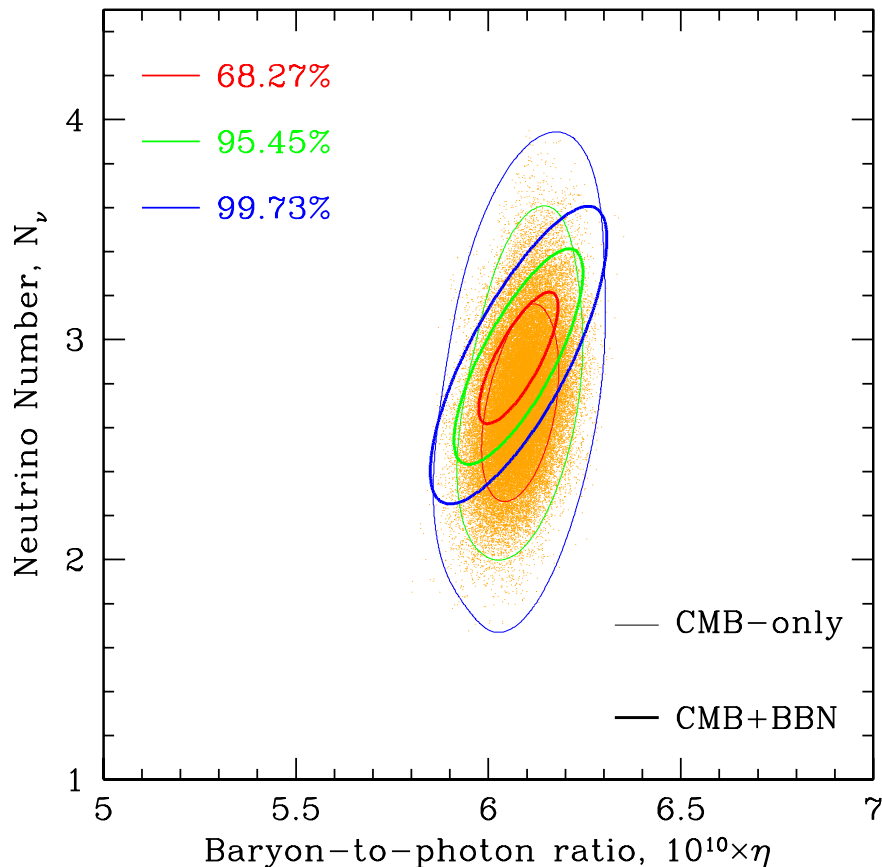


FIG. 6. The 2D likelihood function contours derived from the *Planck* Markov Chain Monte Carlo **base\_nnu\_yhe** [113], marginalized over the CMB  $Y_p$  (points). Thin contours are for CMB data only, while thick contours use the BBN  $Y_p(\eta)$  relation, assuming no observational constraints on the light elements. We see that that whereas in the CMB-only case  $N_\nu$  and  $\eta$  are almost uncorrelated, in the CMB+BBN case a stronger correlation emerges.



Turning to the effects of  $N_\nu$  on BBN, eqs. (1) – (3) show that increasing the number of neutrino flavors leads to an increased Hubble parameter which in turn leads to an increased freeze-out temperature,  $T_f$ . Since the neutron-to-proton ratio at freeze-out scales as  $(n/p) \simeq e^{-\Delta m/T_f}$ , higher  $T_f$  leads to higher  $(n/p)$  and thus higher  $Y_p$  [122]. As a consequence, one can establish an upper bound to the number of neutrinos [123] if in addition one has a lower bound on the baryon-to-photon ratio [25] as the helium abundance also scales monotonically with  $\eta$ . The dependence of the helium mass fraction  $Y$  on both  $\eta$  and  $N_\nu$  can be seen in Figure 7 where we see the calculated value of  $Y$  for  $N_\nu = 2, 3$  and 4 as depicted by the blue, green and red curves respectively. In the Figure, one clearly sees not only the monotonic growth of  $Y$  with  $\eta$ , but also the strong sensitivity of  $Y$  with  $N_\nu$ . The importance of a lower bound on  $\eta$  (or better yet fixing  $\eta$ ) is clearly apparent in setting an upper bound on  $N_\nu$ . Prior to CMB determinations of  $\eta$ , the lower bound on  $\eta$  could be set using a combination of D and  $^3\text{He}$  observations enabling a limit of  $N_\nu < 4$  [124] given the estimated uncertainties in  $Y_p$  at the time. More aggressive estimates of an upper bound on the helium mass fraction led to tighter bounds on  $N_\nu$  [1, 109, 125]. The bounds on  $N_\nu$  became more rigorous when likelihood techniques were introduced [5, 57, 109, 126–129].

While the dependence of  $Y_p$  on  $N_\nu$  is well documented, we also see from Fig. 7, there is a non-negligible effect on D and  $^7\text{Li}$  from changes in  $N_\nu$  [5]. In particular, while the sensitivity of D to  $N_\nu$  is not as great as that of  $Y_p$ , the deuterium abundance is measured much more accurately and as a result the constraint on  $N_\nu$  is now due to both abundance determinations as can be discerned from Table V.

By marginalizing over the baryon density, we can form 1-d likelihood functions for  $N_\nu$ . These are shown in Figure 8. In the left panel, we show the CMB-only result by the blue curve. Recall that this uses no BBN correlation between the baryon density and helium abundance. While the peak of the likelihood for this case is lowest of the cases considered ( $N_\nu = 2.67$ ) its uncertainty ( $\approx 0.30$ ) makes it consistent with the Standard Model. The position of the peak of the likelihood function is given in Table V for this case as well as the other cases considered in the Figures. In contrast the red curve shows the limit we obtain

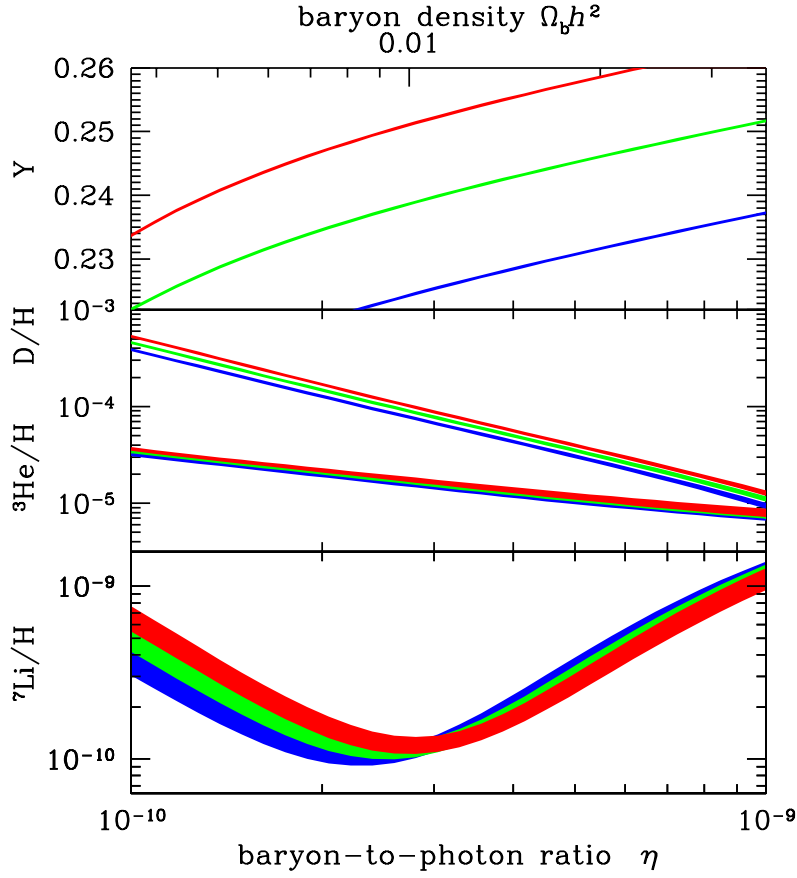


FIG. 7. The sensitivity of the light element predictions to the number of neutrino species, similar to Figure 1. Here, abundances shown by blue, green, and red bands correspond to calculated abundances assuming  $N_\nu = 2, 3$  and 4 respectively.

purely from matching the BBN calculations with the observed abundances of helium and deuterium. In this case, the fact that the peak of the likelihood function is at  $N_\nu = 2.85$  can be traced directly to the fact that the central helium abundance is  $Y_p = 0.2449$ . Given the sensitivity of  $Y_p$  to  $N_\nu$  found in Eq. 13, the drop in  $N_\nu$  from the Standard Model value of 3.0, compensates for a helium abundance below the Standard Model prediction closer to 0.247. Nevertheless, the uncertainty again places the Standard Model within  $1\sigma$  of the distribution peak. The remaining cases displayed (in green) correspond to combining the CMB data with BBN. There are 4 green curves in the left panel and these have been isolated in the right panel for better clarity. As one can see, once one combines the BBN relation between helium and the baryon density, the actual abundance determinations have only a

secondary effect in determining  $N_\nu$  which takes values between 2.88 and 2.91. Using the CMB, BBN and the abundances of both D and  $^4\text{He}$ , yields the tightest constraint on the number of neutrino flavors  $N_\nu = 2.88 \pm 0.16$ , again consistent with the Standard Model<sup>5</sup>. It is interesting to note, that because of the drop in  $Y_p$  in the most recent analysis [39], the 95% CL upper limit on  $N_\nu$  is 3.20.

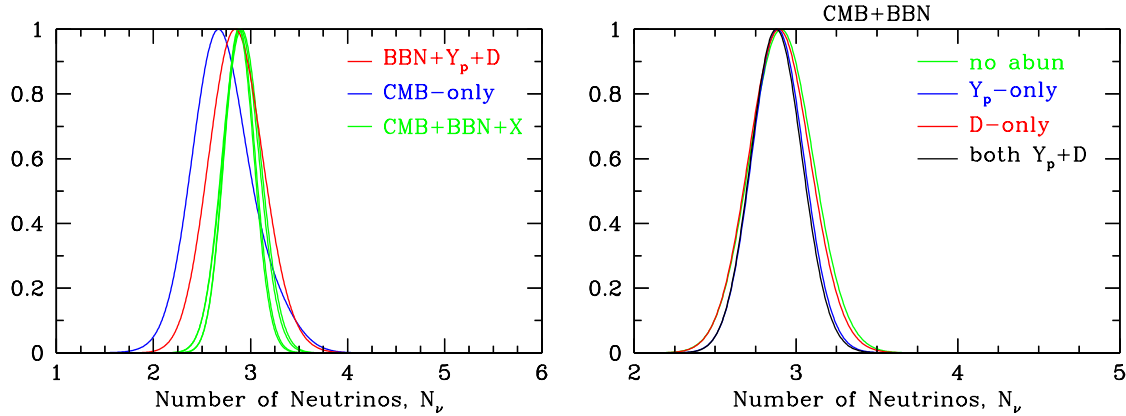


FIG. 8. The marginalized distributions for the number of neutrinos, given different combinations of observational constraints. The left panel shows the likelihood function the case where only CMB data is used (blue), only BBN and abundance data is used (red) and when a combination of BBN and CMB data is used (green). The four green curves are shown again in the right panel for better clarity.

It is also possible to marginalize over the number of neutrino flavors and produce a 1-d likelihood function for  $\eta_{10}$  as shown in Figure 9. In the left panel, the broad distribution shown in red corresponds to the BBN plus abundance data constraint using no information from the CMB. Here the baryon density is primarily determined by the D/H abundance. When the CMB is added, the uncertainty in  $\eta$  drops dramatically (from 0.23 to 0.06 or 0.07) independent of whether abundance data is used. The 5 green curves are almost indistinguishable and are shown in more detail in the right panel. Once again the peak of the likelihood distributions are given in Table V. The values of  $\eta$  are slightly lower than the Standard Model results discussed above. This is due to the additional freedom in the

<sup>5</sup> Of all the cases considered, the one that can best be compared with the results presented by the *Planck* collaboration [6] is the case CMB+BBN+D. We find  $N_{\text{eff}} = 2.94 \pm 0.38(2\sigma)$  while they quote  $N_{\text{eff}} = 2.91 \pm 0.37$ . While we obtain similar results to other cases, direct comparison is complicated not only by the slight difference in the  $\eta - Y$  relation due to different BBN codes, but also by the adopted value for primordial  $^4\text{He}$ .

likelihood distribution afforded by the additional parameter,  $N_\nu$ .

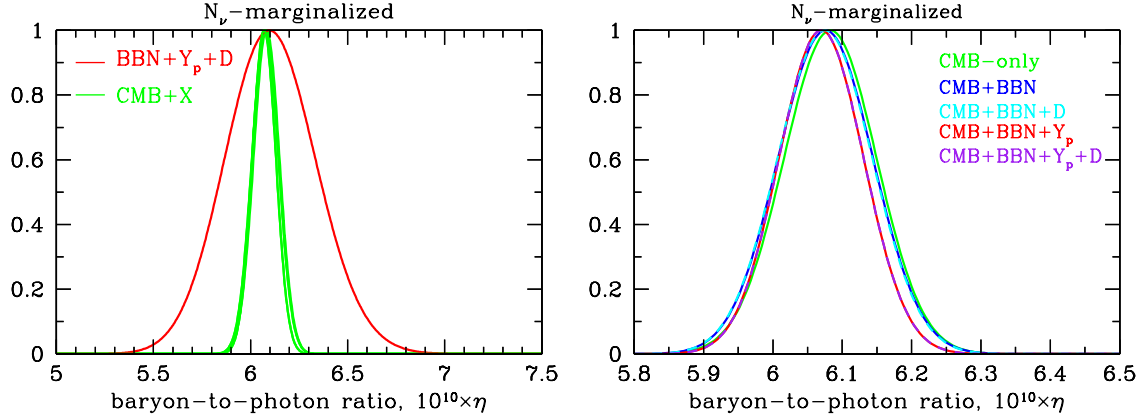


FIG. 9. The marginalized distributions for the baryon to photon ratio ( $\eta$ ), given different combinations of observational constraints.

For completeness, we also show 2-d likelihood contours in the  $\eta_{10} - N_\nu$  plane in Fig. 10. The three panels show the effect of the constraints imposed by the helium and deuterium abundances. In the first panel, only the helium abundance constraints are applied. The thinner open curves are based on BBN alone. They appear open as the helium abundance alone is a poor baryometer as has been noted several times already. Without the CMB, the helium abundance data can produce an upper limit on  $N_\nu$  of about 4 and depends weakly on the value of  $\eta$ . When the CMB data is applied, we obtain the thicker closed contours. The precision determination of  $\eta$  from the anisotropy spectrum correspondingly produces a very tight limit in  $N_\nu$ . Here, we see clearly that the Standard Model value of  $N_\nu = 3$  falls well within the 68% CL contour.

The next panel of Figure 10 shows the likelihood contours using the deuterium abundance data. Once again, the thin open curves are based on BBN alone. In this case, they appear open as the deuterium abundance is less sensitive to  $N_\nu$ , though we do note that the contours are not vertical and do show some dependence on  $N_\nu$  as discussed above. In contrast to  $^4\text{He}$ , for fixed  $N_\nu$ , the deuterium abundance is capable of fixing  $\eta$  relatively precisely. Of course when the CMB data is added, the open contours collapse once again into a series of narrow ellipses.

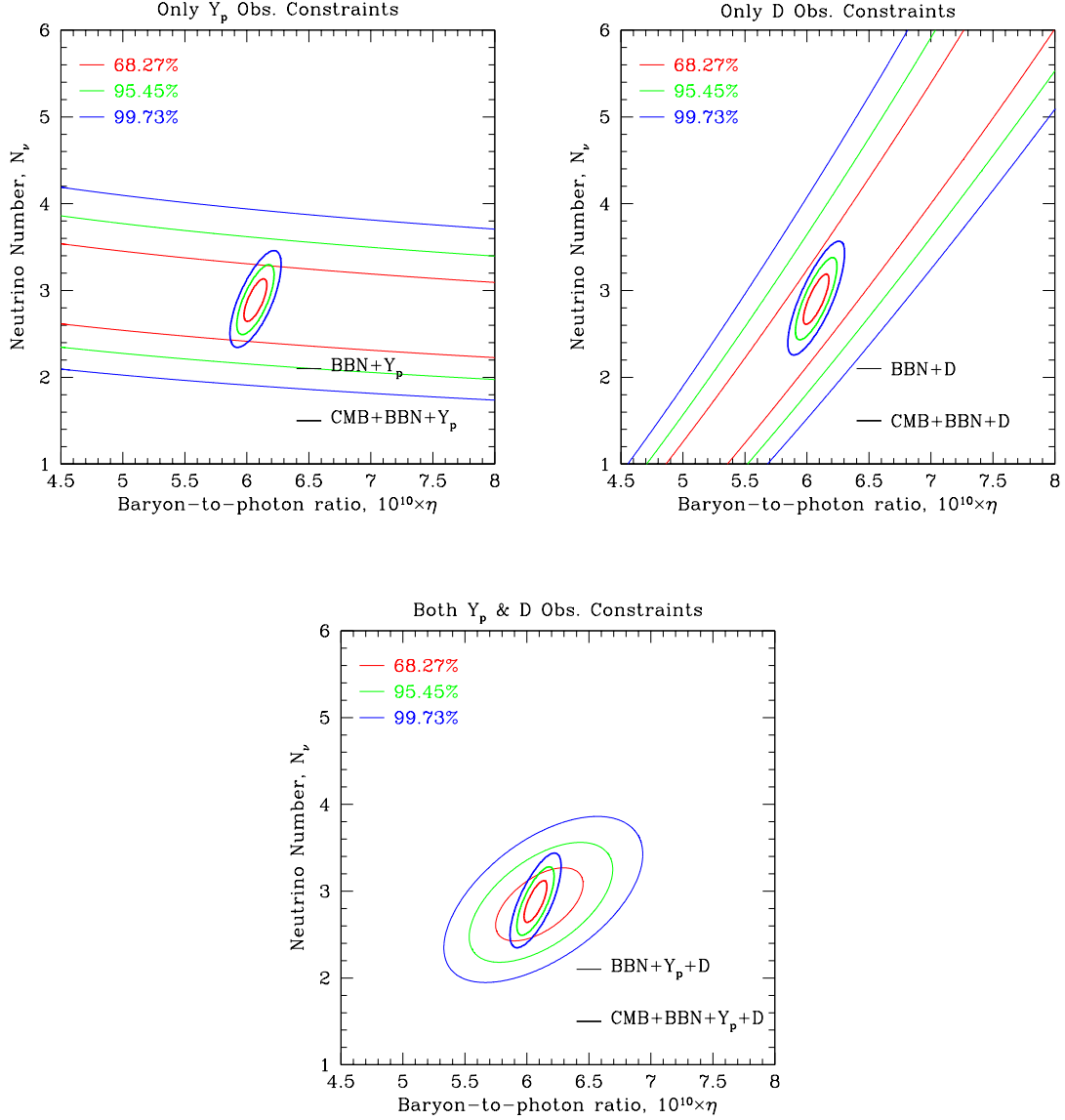


FIG. 10. The resulting 2-dimensional likelihood functions for the baryon to photon ratio ( $\eta$ ) and the number of neutrinos ( $N_\nu$ ), marginalized over the helium mass fraction  $Y_p$ , assuming different combinations of observational constraints on the light elements.

The last panel of Figure 10 shows the likelihood contours using both the  $^4\text{He}$  and D/H data. In this case, even without any CMB input, we are able to obtain reasonably strong constraints on both  $\eta$  and  $N_\nu$ , as seen by the thin and larger ellipses. When the CMB data is added we recover the tight constraints which are qualitatively similar to those in the previous two panels.

Finally, above in Figure 6, we show the 2-dimensional likelihood function using either CMB only (the thin outer curves which trace the density of models results of the Monte-

Carlo), or the combination of CMB and BBN (tighter and thicker curves). In the latter case, no abundance data is used.

## VII. DISCUSSION

Big bang cosmology can be said to have gone full circle. The prediction of the CMB was made in the context of the development of BBN and of what became Big Bang Cosmology [130]. Now, the CMB is providing the precision necessary to make accurate prediction of the light element abundances in SBBN. In the Standard Model with  $N_\nu = 3$ , BBN makes relatively accurate predictions of the light element abundance as displayed by the thickness of the bands in Figure 1. These can be compared directly (or convoluted through a likelihood function) to the observational determination of the light element abundances. The agreement between the theoretical predictions and the abundance D/H is stunning. Recent developments in the determination of D/H has produced unparalleled accuracy [40]. This agreement is seen instantly when comparing the likelihood functions of the observations with that of the predictions of BBN using CMB data as seen in the second panel of Figure 3. The helium data has also seen considerable progress. New data utilizing a near infrared emission line [36] has led to a marked drop in the uncertainty of the extrapolated primordial  $^4\text{He}$  abundance [39]. While the error remains large compared with the precision of the BBN prediction, the agreement between theory and observation is still impressive.

Is two out of three okay? Despite the success of the BBN predictions for  $^4\text{He}$  and D/H, there remains a problem with  $^7\text{Li}$  [19, 114]. The predicted primordial abundance is about a factor of three higher than the abundance determined from absorption lines seen in a population of low metallicity halo stars. The primordial abundance has since 1981 been associated with a narrow plateau [88] of abundance measurements. Recently, the extent of this plateau has been called into question as a significant amount of downward dispersion is seen at very low metallicity ( $[\text{Fe}/\text{H}] < -3$ ) [94, 95]. If stellar depletion is the explanation of the discrepancy between the plateau value and the BBN prediction, it remains to be explained why there are virtually no low metallicity stars with abundances above the plateau for all metallicities below  $[\text{Fe}/\text{H}] < -1.5$ . If depletion is not the answer, then perhaps the lithium discrepancy points to new physics beyond the Standard Model.

In this review, we have presented the latest combined analysis of BBN predictions using

raw CMB data provided by *Planck* [6, 113]. He have constructed a series of likelihood function which include various combinations of the CMB, the BBN relation between the baryon density and the helium abundance, and various combinations of  $^4\text{He}$  and D/H data. We presented detailed fits and sensitivities of the light element abundances to the various input parameters as well as the dominant input nuclear rates. This allowed us to make relatively precise comparisons between theory and observations in standard BBN. The uncertainty in the prediction of  $^4\text{He}$  remains dominated by the uncertainty in the neutron mean life. We also considered a one-parameter extension of SBBN, allowing the number of relativistic degrees of freedom characterized by the number of neutrino flavors to differ from the Standard Model value of  $N_\nu = 3$ . Despite the additional freedom, strong constraints on  $\eta$  and  $N_\nu$  were derived. When all abundance data is used in conjunction with BBN and CMB data, we obtain a 95% CL upper limit of  $N_\nu < 3.2$ . As one of the deepest probes in Big Bang Cosmology, BBN continues to thrive.

Going beyond 2015, we expect further improvements in the data which will better test the Standard Model. More high resolution data on  $^4\text{He}$  emission lines could yield a further drop in the uncertainty in primordial helium. One should recall that there are still only a little over a dozen objects which are well described by models of the emission line regions. That said, there are less than half a dozen quasar absorption systems which yield high precision D/H abundances. Moreover, the nuclear physics uncertainties in D/H now dominate the error budget. Thus there is strong motivation for future measurements of the rates most important for deuterium:  $d(p, \gamma)^3\text{He}$ , as well as  $d(d, n)^3\text{He}$ ,  $d(d, n)t$ , and  $n(p, \gamma)^3\text{He}$  [131, 132]. We can be hopeful that future measurements lead to a reduction in the already small uncertainty in primordial D/H; futuristically, there is hope of detecting cosmological 92 cm deuterium hyperfine lines that would probe D/H at extremely high redshift [133]. Lastly, we can be certain to expect updated results from the CMB data when the *Planck* collaboration produces its final data release.

## APPENDIX

In order to reproduction the likelihoods, we need order 3 and 4 (skewness and kurtosis) terms in the multi-dimensional expansion.

In 1D, this expansion looks like:

$$\mathcal{L}(x) = \frac{\exp\left\{-\frac{1}{2}z^2\right\}}{\sqrt{2\pi}\sigma} \times [1. + SH_3(z) + KH_4(z)], \quad (29)$$

where  $z = (x - \mu)/\sigma$ ,  $\mu$  is the mean value and  $\sigma$  is the standard deviation and  $S$  and  $K$  are the skewness and kurtosis coefficients needed to adequately describe the distribution via a Hermite polynomial expansion. The skewness and kurtosis coefficients are proportional to the Markov Chain average of the respective Hermite polynomials ( $S \propto \langle H_3(x) \rangle$  and  $K \propto \langle H_4(z) \rangle$ ). In multiple dimensions, the simple gaussian base distribution is replaced with the fully correlated multi-dimensional gaussian:

$$\begin{aligned} \mathcal{L}(\vec{x}) = & \frac{\exp\left\{-\frac{1}{2}(\vec{x} - \vec{\mu})^T \mathcal{C}^{-1}(\vec{x} - \vec{\mu})\right\}}{\sqrt{(2\pi)^d \text{Det}(\mathcal{C})}} \\ & \times \left[ 1. + \sum_{n,m,p=0}^3 S_{nmp,ijk} H_n(z_i) H_m(z_j) H_p(z_k) \delta_{3,n+m+p} \right. \\ & \left. + \sum_{n,m,p,q=0}^4 K_{nmpq,ijkl} H_n(z_i) H_m(z_j) H_p(z_k) H_q(z_l) \delta_{4,n+m+p+q} \right]. \end{aligned} \quad (30)$$

## ACKNOWLEDGMENTS

It is a pleasure to thank our recent BBN collaborators Nachiketa Chakraborty, John Ellis, Doug Friedel, Athol Kemball, Lloyd Knox, Feng Luo, Marius Millea, Tijana Prodanović, Vassilis Spanos, and Gary Steigman. The work of R.H.C was supported by the National Science Foundation under Grant No. PHY-1430152 (JINA Center for the Evolution of the Elements). The work of K.A.O. was supported in part by DOE grant DE-SC0011842 at the University of Minnesota. The work of B.D.F. and T.H.Y. was partially supported by the U.S. National Science Foundation Grant PHY-1214082.

- 
- [1] T. P. Walker, G. Steigman, D. N. Schramm, K. A. Olive and H. S. Kang, *Astrophys. J.* **376** (1991) 51.
  - [2] K. A. Olive, G. Steigman and T. P. Walker, *Phys. Rept.* **333**, 389 (2000) [astro-ph/9905320]; B. D. Fields and K. A. Olive, *Nucl. Phys.* **A777**, 208 (2006); B. D. Fields, P. Molaro and S. Sarkar, *Chin. Phys. C* **38** (2014) [arXiv:1412.1408 [astro-ph.CO]]; G. Steigman, *Ann. Rev. Nucl. Part. Sci.* **57**, 463 (2007) [arXiv:0712.1100 [astro-ph]].



- [3] F. Iocco, G. Mangano, G. Miele, O. Pisanti and P. D. Serpico, *Phys. Rept.* **472**, 1 (2009) [arXiv:0809.0631 [astro-ph]].
- [4] O. Pisanti, A. Cirillo, S. Esposito, F. Iocco, G. Mangano, G. Miele and P. D. Serpico, *Comput. Phys. Commun.* **178**, 956 (2008) [arXiv:0705.0290 [astro-ph]].
- [5] R. H. Cyburt, B. D. Fields and K. A. Olive, *Astropart. Phys.* **17** (2002) 87 [arXiv:astro-ph/0105397].
- [6] P. A. R. Ade *et al.* [Planck Collaboration], arXiv:1502.01589 [astro-ph.CO].
- [7] C. Angulo, M. Arnould, M. Rayet, P. Descouvemont, D. Baye, C. Leclercq-Willain, A. Coc and S. Barhoumi *et al.*, *Nucl. Phys. A* **656**, 3 (1999).
- [8] K. M. Nollett and S. Burles, *Phys. Rev. D* **61**, 123505 (2000) [astro-ph/0001440]; S. Burles, K. M. Nollett and M. S. Turner, *Astrophys. J.* **552**, L1 (2001) [astro-ph/0010171].
- [9] E. Vangioni-Flam, A. Coc and M. Casse, *Astron. Astrophys.* **360**, 15 (2000) [astro-ph/0002248].
- [10] R. H. Cyburt, B. D. Fields and K. A. Olive, *New Astron.* **6** (1996) 215 [arXiv:astro-ph/0102179].
- [11] A. Coc, E. Vangioni-Flam, M. Cassé and M. Rabiet, *Phys. Rev.* **D65** (2002) 043510 [arXiv:astro-ph/0111077].
- [12] R. H. Cyburt, B. D. Fields and K. A. Olive, *Phys. Lett. B* **567**, 227 (2003) [astro-ph/0302431].
- [13] A. Coc, E. Vangioni-Flam, P. Descouvemont, A. Adahchour and C. Angulo, *Ap. J.* **600** (2004) 544 [arXiv:astro-ph/0309480].
- [14] R. H. Cyburt, *Phys. Rev. D* **70** (2004) 023505 [arXiv:astro-ph/0401091].
- [15] P. Descouvemont, A. Adahchour, C. Angulo, A. Coc and E. Vangioni-Flam, *ADNDT* **88** (2004) 203 [arXiv:astro-ph/0407101];
- [16] A. Cuoco, F. Iocco, G. Mangano, G. Miele, O. Pisanti and P. D. Serpico, *Int. J. Mod. Phys. A* **19** (2004) 4431 [arXiv:astro-ph/0307213]; P. D. Serpico, S. Esposito, F. Iocco, G. Mangano, G. Miele and O. Pisanti, *JCAP* **0412**, 010 (2004) [arXiv:astro-ph/0408076];
- [17] A. Coc, S. Goriely, Y. Xu, M. Saimpert and E. Vangioni, *Astrophys. J.* **744**, 158 (2012) [arXiv:1107.1117 [astro-ph.CO]].
- [18] B. S. N. Singh *et al.*, *Phys. Rev. Lett.* **93**, 262503 (2004) [arXiv:nucl-ex/0407017]; G. Gyürky *et al.*, *Phys. Rev. C* **75**, 035805 (2007) [arXiv:nucl-ex/0702003]; F. Confortola *et al.*, *Phys. Rev. C* **75**, 065803 (2007) [arXiv:0705.2151];

- T. A. D. Brown *et al.*, Phys. Rev. C **76**, 055801 (2007) [arXiv:0710.1279].
- [19] R. H. Cyburt, B. D. Fields and K. A. Olive, JCAP **0811**, 012 (2008) [arXiv:0808.2818 [astro-ph]].
- [20] Y. Xu, K. Takahashi, S. Goriely, M. Arnould, M. Ohta and H. Utsunomiya, Nucl. Phys. A **918**, 61 (2013) [arXiv:1310.7099 [nucl-th]].
- [21] A. Coc, J. -P. Uzan and E. Vangioni, arXiv:1403.6694 [astro-ph.CO].
- [22] C. J. Christensen, A. Nielsen, A. Bahnsen, W. K. Brown and B. M. Rustad, Phys. Rev. D **5**, 1628 (1972).
- [23] L. N. Bondarenko, V. V. Kurguzov, Yu. A. Prokofev, E. V. Rogov and P. E. Spivak, Pisma Zh. Eksp. Teor. Fiz. **28**, 328 (1978) [JETP Lett. **28**, 303 (1978)].
- [24] J. Byrne, J. Morse, K. F. Smith, F. Shaikh, K. Green and G. L. Greene, Phys. Lett. B **92**, 274 (1980).
- [25] K. A. Olive, D. N. Schramm, G. Steigman, M. S. Turner and J. -M. Yang, Astrophys. J. **246**, 557 (1981).
- [26] W. Mampe, P. Ageron, C. Bates, J. M. Pendlebury and A. Steyerl, Phys. Rev. Lett. **63**, 593 (1989).
- [27] A. Serebrov, V. Varlamov, A. Kharitonov, A. Fomin, Y. .Pokotilovski, P. Geltenbort, J. Butterworth and I. Krasnoschekova *et al.*, Phys. Lett. B **605**, 72 (2005) [nucl-ex/0408009].
- [28] G. J. Mathews, T. Kajino and T. Shima, Phys. Rev. D **71**, 021302 (2005) [astro-ph/0408523].
- [29] K. A. Olive *et al.* [Particle Data Group Collaboration], Chin. Phys. C **38**, 090001 (2014).
- [30] K. A. Olive and E. D. Skillman, New Astron. **6** (2001) 119 [arXiv:astro-ph/0007081]; K. A. Olive and E. D. Skillman, *ApJ* **617** (2004) 29 [arXiv:astro-ph/0405588].
- [31] E. Aver, K. A. Olive and E. D. Skillman, JCAP **1005**, 003 (2010) [arXiv:1001.5218 [astro-ph.CO]]; E. Aver, K. A. Olive and E. D. Skillman, JCAP **1103**, 043 (2011) [arXiv:1012.2385 [astro-ph.CO]].
- [32] E. Aver, K. A. Olive and E. D. Skillman, JCAP **1204**, 004 (2012) [arXiv:1112.3713 [astro-ph.CO]].
- [33] Y. I. Izotov, T. X. Thuan and V. A. Lipovetsky, Astrophys. J. **435**, 647 (1994); Y. I. Izotov, T. X. Thuan and V. A. Lipovetsky, Astrophys. J. Suppl. **108**, 1 (1997);
- [34] Y. I. Izotov, T. X. Thuan and G. Stasińska, Astrophys. J. **662**, 15 (2007) [arXiv:astro-ph/0702072].

- [35] Y. I. Izotov, G. Stasinska and N. G. Guseva, *Astron. Astrophys.* **558**, A57 (2013) [arXiv:1308.2100 [astro-ph.CO]].
- [36] Y. I. Izotov, T. X. Thuan and N. G. Guseva, *Mon. Not. Roy. Astron. Soc.* **445**, 778 (2014) [arXiv:1408.6953 [astro-ph.CO]].
- [37] R. L. Porter, G. J. Ferland, P. J. Storey and M. J. Detisch, *Mon. Not. Roy. Astron. Soc.* **425**, L28 (2012) arXiv:1206.4115 [astro-ph.CO]; R. L. Porter, G. J. Ferland, P. J. Storey and M. J. Detisch, *Mon. Not. Roy. Astron. Soc.* **433**, L89 (2013) arXiv:1303.5115 [astro-ph.CO].
- [38] E. Aver, K. A. Olive, R. L. Porter and E. D. Skillman, *JCAP* **1311**, 017 (2013) [arXiv:1309.0047 [astro-ph.CO]].
- [39] E. Aver, K. A. Olive and E. D. Skillman, arXiv:1503.08146 [astro-ph.CO].
- [40] R. Cooke, M. Pettini, R. A. Jorgenson, M. T. Murphy and C. C. Steidel, *Ap. J.* **781**, 31 (2014) [arXiv:1308.3240 [astro-ph.CO]].
- [41] R. H. Cyburt, B. D. Fields and K. A. Olive, *Phys. Rev. D* **69**, 123519 (2004) [arXiv:astro-ph/0312629].
- [42] R. N. Boyd, C. R. Brune, G. M. Fuller and C. J. Smith, *Phys. Rev. D* **82**, 105005 (2010) [arXiv:1008.0848 [astro-ph.CO]].
- [43] R. H. Cyburt and M. Pospelov, *Int. J. Mod. Phys. E* **21**, 1250004 (2012) [arXiv:0906.4373 [astro-ph.CO]].
- [44] N. Chakraborty, B. D. Fields and K. A. Olive, *Phys. Rev. D* **83**, 063006 (2011) [arXiv:1011.0722 [astro-ph.CO]].
- [45] C. Broggini, L. Canton, G. Fiorentini and F. L. Villante, *JCAP* **1206**, 030 (2012) [arXiv:1202.5232 [astro-ph.CO]].
- [46] S. Vauclair, and C. Charbonnel, *Ap. J.* **502** (1998) 372 [arXiv:astro-ph/9802315]; M. H. Pinsonneault, T. P. Walker, G. Steigman and V. K. Narayanan, *Ap. J.* **527** (1998) 180 [arXiv:astro-ph/9803073]; M. H. Pinsonneault, G. Steigman, T. P. Walker, and V. K. Narayanan, *Ap. J.* **574** (2002) 398 [arXiv:astro-ph/0105439]; O. Richard, G. Michaud and J. Richer, *Astrophys. J.* **619**, 538 (2005) [arXiv:astro-ph/0409672]; A. J. Korn *et al.*, *Nature* **442**, 657 (2006) [arXiv:astro-ph/0608201]; A. E. García Pérez, S., Inoue, W. Aoki, and S. G. Ryan, in *Precision Spectroscopy in Astrophysics*, Proceedings of the ESO/Lisbon/Aveiro Conference, 9 (2008).

- [47] M. Pospelov and N. Afshordi, arXiv:1208.0793 [astro-ph.CO]; M. Kusakabe and M. Kawasaki, Mon. Not. Roy. Astron. Soc. **446**, 1597 (2015) [arXiv:1404.3485 [astro-ph.CO]].
- [48] K. Jedamzik, Phys. Rev. D **70** (2004) 063524 [arXiv:astro-ph/0402344]; K. Jedamzik, Phys. Rev. D **70** (2004) 083510 [arXiv:astro-ph/0405583]; M. Kawasaki, K. Kohri and T. Moroi, Phys. Lett. B **625** (2005) 7 [arXiv:astro-ph/0402490]; Phys. Rev. D **71** (2005) 083502 [arXiv:astro-ph/0408426];
- [49] For a reviews see: K. Jedamzik and M. Pospelov, New J. Phys. **11**, 105028 (2009) [arXiv:0906.2087 [hep-ph]]; and M. Pospelov and J. Pradler, Ann. Rev. Nucl. Part. Sci. **60**, 539 (2010) [arXiv:1011.1054 [hep-ph]].
- [50] R. H. Cyburt, J. Ellis, B. D. Fields, F. Luo, K. A. Olive and V. C. Spanos, JCAP **1010** (2010) 032 [arXiv:1007.4173 [astro-ph.CO]]; R. H. Cyburt, J. Ellis, B. D. Fields, F. Luo, K. A. Olive and V. C. Spanos, JCAP **1212**, 037 (2012) [arXiv:1209.1347 [astro-ph.CO]]; R. H. Cyburt, J. Ellis, B. D. Fields, F. Luo, K. A. Olive and V. C. Spanos, JCAP **1305**, 014 (2013) [arXiv:1303.0574 [astro-ph.CO]].
- [51] V. Poulin and P. D. Serpico, Phys. Rev. Lett. **114**, no. 9, 091101 (2015) [arXiv:1502.01250 [astro-ph.CO]].
- [52] O. Erken, P. Sikivie, H. Tam and Q. Yang, Phys. Rev. Lett. **108**, 061304 (2012) [arXiv:1104.4507 [astro-ph.CO]]; M. Kusakabe, A. B. Balantekin, T. Kajino and Y. Pehlivan, Phys. Lett. B **718**, 704 (2013) [arXiv:1202.5603 [astro-ph.CO]].
- [53] V. F. Dmitriev, V. V. Flambaum and J. K. Webb, Phys. Rev. D **69**, 063506 (2004) [arXiv:astro-ph/0310892]; J. C. Berengut, V. V. Flambaum and V. F. Dmitriev, Phys. Lett. B **683**, 114 (2010) [arXiv:0907.2288 [nucl-th]].
- [54] A. Coc, N. J. Nunes, K. A. Olive, J. P. Uzan and E. Vangioni, Phys. Rev. D **76**, 023511 (2007) [arXiv:astro-ph/0610733]; A. Coc, P. Descouvemont, K. A. Olive, J. -P. Uzan and E. Vangioni, Phys. Rev. D **86**, 043529 (2012) [arXiv:1206.1139 [astro-ph.CO]].
- [55] R. Cayrel *et al.*, Astron. Astrophys. **473**, L37 (2007) [arXiv:0708.3819 [astro-ph]]; A. E. G. Perez, W. Aoki, S. Inoue, S. G. Ryan, T. K. Suzuki and M. Chiba, Astron. Astrophys. **504**, 213 (2009) [arXiv:0909.5163 [astro-ph.SR]]; M. Steffen, R. Cayrel, P. Bonifacio, H. G. Ludwig and E. Caffau, IAU Symposium, 265, 23 (2010) [arXiv:0910.5917 [astro-ph.SR]].
- [56] K. Lind, J. Melendez, M. Asplund, R. Collet and Z. Magic, Astron. Astrophys. **544**, A96 (2013) [arXiv:1305.6564 [astro-ph.SR]].

- [57] S. Sarkar, Rept. Prog. Phys. **59**, 1493 (1996) [hep-ph/9602260]; R. H. Cyburt, B. D. Fields, K. A. Olive and E. Skillman, Astropart. Phys. **23**, 313 (2005) [astro-ph/0408033].
- [58] J. Bernstein, L. S. Brown and G. Feinberg, *Rev. Mod. Phys.* **61** (1989) 25.
- [59] V. F. Mukhanov, Int. J. Theor. Phys. **43**, 669 (2004) [astro-ph/0303073].
- [60] R. V. Wagoner, Astrophys. J. Supp. **18**, 247 (1969).
- [61] D. A. Dicus, E. W. Kolb, A. M. Gleeson, E. C. G. Sudarshan, V. L. Teplitz and M. S. Turner, Phys. Rev. D **26**, 2694 (1982). C. J. Smith and G. M. Fuller, Phys. Rev. D **81**, 065027 (2010) [arXiv:0905.2781 [astro-ph.CO]].
- [62] P. J. Kernan, UMI-94-01290.
- [63] D. Seckel, hep-ph/9305311; R. E. Lopez, M. S. Turner and G. Gyuk, Phys. Rev. D **56**, 3191 (1997) [astro-ph/9703065].
- [64] S. Ando, R. H. Cyburt, S. W. Hong and C. H. Hyun, Phys. Rev. C **74**, 025809 (2006) [nucl-th/0511074].
- [65] R. T. Rood, T. L. Wilson, and G. Steigman, Astrophys. J. **227**, 97 (1979).
- [66] D. Galli, F. Palla, F. Ferrini, U. Penco, Astrophys. J. **443**, 536 (1995); K. A. Olive, R. T. Rood, D. N. Schramm, J. W. Truran and E. Vangioni-Flam, Astrophys. J. **444**, 680 (1995) [astro-ph/9410058]; S. T. Scully, M. Casse, K. A. Olive, D. N. Schramm, J. Truran and E. Vangioni-Flam, Astrophys. J. **462**, 960 (1996) [astro-ph/9508086]; D. S. P. Dearborn, G. Steigman and M. Tosi, Astrophys. J. **465**, 887 (1996) [astro-ph/9601117]; S. Scully, M. Casse, K. A. Olive and E. Vangioni-Flam, Astrophys. J. **476**, 521 (1997) [astro-ph/9607106]; D. Galli, L. Stanghellini, M. Tosi and F. Palla, Astrophys. J. **477**, 218 (1997) [astro-ph/9609184]; K. A. Olive, D. N. Schramm, S. T. Scully and J. W. Truran, Astrophys. J. **479**, 752 (1997) [astro-ph/9610039]; T. M. Bania, R. T. Rood, and D. S. Bania, Nature **415**, 54 (2002); E. Vangioni-Flam, K. A. Olive, B. D. Fields and M. Casse, Astrophys. J. **585**, 611 (2003) [astro-ph/0207583].
- [67] M. Peimbert and S. Torres-Peimbert, Astrophys. J. **193**, 327 (1974).
- [68] M. Peimbert, V. Luridiana and A. Peimbert, Astrophys. J. **666**, 636 (2007) [arXiv:astro-ph/0701580].
- [69] R. I. Epstein, J. M. Lattimer and D. N. Schramm, Nature **263**, 198 (1976); T. Prodanović and B. D. Fields, Astrophys. J. **597**, 48 (2003) [astro-ph/0307183].
- [70] H. Reeves, J. Audouze, W. A. Fowler and D. N. Schramm, Astrophys. J. **179**, 909 (1973).

- [71] J. R. Gott, III, J. E. Gunn, D. N. Schramm and B. M. Tinsley, *Astrophys. J.* **194**, 543 (1974).
- [72] J. L. Linsky, *Space Sci. Rev.* **106**, 49 (2003) [astro-ph/0309099]; H. W. Moos, K. R. Sembach, A. Vidal-Madjar, D. G. York, S. D. Friedman, G. Hebrard, J. W. Kruk and N. Lehner *et al.*, *Astrophys. J. Suppl.* **140**, 3 (2002) [astro-ph/0112519]; B. E. Wood, J. L. Linsky, G. Hebrard, G. M. Williger, H. W. Moos and W. P. Blair, *Astrophys. J.* **609**, 838 (2004) [astro-ph/0403606]; T. Prodanović, G. Steigman and B. D. Fields, *Mon. Not. Roy. Astron. Soc.* **406**, 1108 (2010) [arXiv:0910.4961 [astro-ph.GA]].
- [73] J. L. Linsky, B. T. Draine, H. W. Moos, E. B. Jenkins, B. E. Wood, C. Oliveira, W. P. Blair and S. D. Friedman *et al.*, *Astrophys. J.* **647**, 1106 (2006) [astro-ph/0608308].
- [74] B. Savage, N. Lehner, A. Fox, B. Wakker and K. Sembach, *Astrophys. J.* **659**, 1222 (2007) [[astro-ph/0701110]].
- [75] J. Audouze and B. M. Tinsley, *Astrophys. J.* **192**, 487 (1974); J.P. Ostriker and B.M. Tinsley, *Astrophys. J.* **201**, L51 (1975); E. Vangioni-Flam and J. Audouze, *Astron. Astrophys.* **193**, 81 (1988); G. Steigman and M. Tosi, *Astrophys. J.* **401**, 150 (1992); E. Vangioni-Flam, K. A. Olive and N. Prantzos, *Astrophys. J.* **427**, 618 (1994) [astro-ph/9310021]; M. G. Edmunds, *Mon. Not. Roy. Astron. Soc.* **270**, L37 (1994); B. D. Fields, *Astrophys. J.* **456**, 478 (1996) [astro-ph/9512044]; S. Scully, M. Casse, K. A. Olive and E. Vangioni-Flam, *Astrophys. J.* **476**, 521 (1997) [astro-ph/9607106]; M. Tosi, G. Steigman, F. Matteucci and C. Chiappini, *Astrophys. J.* **498**, 226 (1998) [astro-ph/9706114]; M. Casse, K. A. Olive, E. Vangioni-Flam and J. Audouze, *New Astron.* **3**, 259 (1998) [astro-ph/9712261]; B. D. Fields, K. A. Olive, J. Silk, M. Casse and E. Vangioni-Flam, *Astrophys. J.* **563**, 653 (2001) [astro-ph/0107389]; G. Steigman, D. Romano and M. Tosi, *Mon. Not. Roy. Astron. Soc.* **378**, 576 (2007) [astro-ph/0703682 [ASTRO-PH]]; E. Vangioni, J. Silk, K. A. Olive and B. D. Fields, *Mon. Not. Roy. Astron. Soc.* **413**, 2987 (2011) [arXiv:1010.5726 [astro-ph.CO]].
- [76] K. A. Olive, P. Petitjean, E. Vangioni and J. Silk, *Mon. Not. Roy. Astron. Soc.* **426**, 1427 (2012) [arXiv:1203.5701 [astro-ph.CO]].
- [77] T. F. Adams, *Astron. Astrophys.* **50**, 461 (1976).
- [78] S. Burles and D. Tytler, *Astrophys. J.* **499**, 699 (1998) [arXiv:astro-ph/9712108]; S. Burles and D. Tytler, *Astrophys. J.* **507**, 732 (1998) [arXiv:astro-ph/9712109].
- [79] J. M. O'Meara, D. Tytler, D. Kirkman, N. Suzuki, J. X. Prochaska, D. Lubin and A. M. Wolfe, *Astrophys. J.* **552**, 718 (2001) [arXiv:astro-ph/0011179]; M. Pettini and

- D. V. Bowen, *Astrophys. J.* **560**, 41 (2001) [arXiv:astro-ph/0104474]; S. A. Levshakov, M. Dessauges-Zavadsky, S. D’Odorico and P. Molaro, *Astrophys. J.* **565**, 696 (2002) [astro-ph/0105529]; D. Kirkman, D. Tytler, N. Suzuki, J. M. O’Meara and D. Lubin, *Astrophys. J. Suppl.* **149**, 1 (2003) [arXiv:astro-ph/0302006]; J. M. O’Meara, S. Burles, J. X. Prochaska, G. E. Prochter, R. A. Bernstein and K. M. Burgess, *Astrophys. J.* **649**, L61 (2006) [arXiv:astro-ph/0608302]; M. Pettini, B. J. Zych, M. T. Murphy, A. Lewis and C. C. Steidel, *MNRAS* **391**, 1499 (2008) [arXiv:0805.0594 [astro-ph]]; R. Srianand, N. Gupta, P. Petitjean, P. Noterdaeme and C. Ledoux, *MNRAS* **405**, 1888 (2010) [arXiv:1002.4620 [astro-ph.CO]]; M. Fumagalli, J. M. O’Meara and J. X. Prochaska, *Science* **334** 1245 (2011) [arXiv:1111.2334 [astro-ph.CO]]; P. Noterdaeme, S. Lopez, V. Dumont, C. Ledoux, P. Molaro and P. Petitjean, *Astron. Astrophys.* **542**, 33 (2012) [arXiv:1205.3777 [astro-ph.CO]].
- [80] M. Pettini and R. Cooke, *Mon. Not. Roy. Astron. Soc.* **425**, 2477 (2012) [arXiv:1205.3785 [astro-ph.CO]].
- [81] S. Reimer-Sørensen, J. K. Webb, N. Crighton, V. Dumont, K. Ali, S. Kotu, M. Bainbridge and M. T. Murphy *et al.*, *Mon. Not. Roy. Astron. Soc.* **447**, 2925 (2015) [arXiv:1412.4043 [astro-ph.CO]].
- [82] R. Khatri and R. A. Sunyaev, *Astron. Lett.* **37**, 367 (2011) [arXiv:1009.3932 [astro-ph.CO]].
- [83] H. Reeves, W. A. Fowler and F. Hoyle, *Nature* **226**, 727 (1970); M. Meneguzzi, J. Audouze, and H. Reeves, *Astron. Astrophys.* **15**, 337 (1971); N. Prantzos, M. Cassé, and E. Vangioni-Flam, *Astrophys. J.* **403**, 630 (1993); R. Ramaty, B. Kozlovsky, R. Lingenfelter, and H. Reeves, *Astrophys. J.* **488**, 730 (1997); B. D. Fields and K. A. Olive, *Astrophys. J.* **516**, 797 (1999) [astro-ph/9809277].
- [84] S. E. Woosley, D. H. Hartmann, R. D. Hoffman and W. C. Haxton, *Astrophys. J.* **356**, 272 (1990); A. Heger, E. Kolbe, W. C. Haxton, K. Langanke, G. Martinez-Pinedo and S. E. Woosley, *Phys. Lett. B* **606**, 258 (2005) [astro-ph/0307546].
- [85] K. A. Olive, N. Prantzos, S. Scully and E. Vangioni-Flam, *Astrophys. J.* **424**, 666 (1994) [astro-ph/9309018].
- [86] A.G.W. Cameron and W.A. Fowler, *Astrophys. J.* **164**, 111 (1971).
- [87] E. Vangioni-Flam, M. Casse, R. Cayrel, J. Audouze, M. Spite and F. Spite, *New Astron.* **4**, 245 (1999) [astro-ph/9811327]; B. D. Fields and K. A. Olive, *New Astron.* **4**, 255 (1999) [astro-ph/9811183].

- [88] F. Spite and M. Spite, *Astron. Astrophys.* **115**, 357 (1982).
- [89] P. Molaro, F. Primas, and P. Bonifacio, *A.A.* **295** (1995) L47 [astro-ph/9503081]; P. Bonifacio and P. Molaro, *Mon. Not. Roy. Astron. Soc.* **285**, 847 (1997) [astro-ph/9611043]; S. G. Ryan, J. E. Norris and T. C. Beers, *Astrophys. J.* **523**, 654 (1999) [arXiv:astro-ph/9903059];
- [90] S. G. Ryan, T. C. Beers, K. A. Olive, B. D. Fields and J. E. Norris, *Astrophys. J.* **530**, L57 (2000).
- [91] P. Bonifacio, P. Molaro, T. Sivarani, R. Cayrel, M. Spite, F. Spite, B. Plez and J. Andersen *et al.*, *Astron. Astrophys.* **462**, 851 (2007). [astro-ph/0610245].
- [92] J. Melendez and I. Ramirez, *Astrophys. J.* **615**, L33 (2004) [astro-ph/0409383].
- [93] A. Hosford, A. E. G. Perez, R. Collet, S. G. Ryan, J. E. Norris and K. A. Olive, *Astron. Astrophys.* **493**, 601 (2009) [arXiv:1004.0863 [astro-ph.SR]]; A. Hosford, S. G. Ryan, A. E. G. Perez, J. E. Norris and K. A. Olive, *Astron. Astrophys.* **511**, 47 (2010) [arXiv:0811.2506 [astro-ph]];
- [94] L. Sbordone, P. Bonifacio, E. Caffau, H.-G. Ludwig, N. T. Behara, J. I. G. Hernandez, M. Steffen and R. Cayrel *et al.*, *Astron. Astrophys.* **522**, A26 (2010) [arXiv:1003.4510 [astro-ph.GA]].
- [95] W. Aoki, P. S. Barklem, T. C. Beers, N. Christlieb, S. Inoue, A. E. G. Perez, J. E. Norris and D. Carollo, *Astrophys. J.* **698**, 1803 (2009) [arXiv:0904.1448 [astro-ph.SR]].
- [96] E. R. Switzer and C. M. Hirata, *Phys. Rev. D* **72**, 083002 (2005) [astro-ph/0507106].
- [97] D. N. Friedel, A. Kemball and B. D. Fields, *Astrophys. J.* **738**, 37 (2011) [arXiv:1106.2471 [astro-ph.CO]].
- [98] M. Asplund, D. L. Lambert, P. E. Nissen, F. Primas and V. V. Smith, *Astrophys. J.* **644**, 229 (2006) [astro-ph/0510636].
- [99] D. N. Spergel *et al.* [WMAP Collaboration], *Astrophys. J. Suppl.* **148**, 175 (2003) [astro-ph/0302209].
- [100] G. Hinshaw *et al.* [WMAP Collaboration], *Astrophys. J. Suppl.* **208** (2013) 19 [arXiv:1212.5226 [astro-ph.CO]];
- [101] E. Komatsu *et al.* [WMAP Science Team Collaboration], *PTEP* **2014**, no. 6, 06B102 (2014) [arXiv:1404.5415 [astro-ph.CO]].



- [102] P. A. R. Ade *et al.* [Planck Collaboration], *Astron. Astrophys.* **571**, A16 (2014) [arXiv:1303.5076 [astro-ph.CO]].
- [103] W. Hu and S. Dodelson, *Ann. Rev. Astron. Astrophys.* **40**, 171 (2002) [astro-ph/0110414]; M. J. White, D. Scott and J. Silk, *Ann. Rev. Astron. Astrophys.* **32**, 319 (1994).
- [104] G. Steigman, *JCAP* **0610**, 016 (2006) [astro-ph/0606206].
- [105] Z. Hou, R. Keisler, L. Knox, M. Millea and C. Reichardt, *Phys. Rev. D* **87**, 083008 (2013) [arXiv:1104.2333 [astro-ph.CO]].
- [106] R. Keisler, C. L. Reichardt, K. A. Aird, B. A. Benson, L. E. Bleem, J. E. Carlstrom, C. L. Chang and H. M. Cho *et al.*, *Astrophys. J.* **743**, 28 (2011) [arXiv:1105.3182 [astro-ph.CO]].
- [107] J. L. Sievers *et al.* [Atacama Cosmology Telescope Collaboration], *JCAP* **1310**, 060 (2013) [arXiv:1301.0824 [astro-ph.CO]].
- [108] L. M. Krauss and P. Romanelli, *Astrophys. J.* **358**, 47 (1990); M. S. Smith, L. H. Kawano and R. A. Malaney, *Astrophys. J. Suppl.* **85**, 219 (1993).
- [109] P. J. Kernan and L. M. Krauss, *Phys. Rev. Lett.* **72**, 3309 (1994) [astro-ph/9402010]; L. M. Krauss and P. J. Kernan, *Phys. Lett. B* **347**, 347 (1995) [astro-ph/9408023].
- [110] N. Hata, R. J. Scherrer, G. Steigman, D. Thomas and T. P. Walker, *Astrophys. J.* **458**, 637 (1996) [astro-ph/9412087].
- [111] B. D. Fields and K. A. Olive, *Phys. Lett. B* **368**, 103 (1996) [hep-ph/9508344]; B. D. Fields, K. Kainulainen, K. A. Olive and D. Thomas, *New Astron.* **1**, 77 (1996) [astro-ph/9603009].
- [112] G. Fiorentini, E. Lisi, S. Sarkar and F. L. Villante, *Phys. Rev. D* **58**, 063506 (1998) [astro-ph/9803177].
- [113] [http://irsa.ipac.caltech.edu/data/Planck/release\\_2/ancillary-data/](http://irsa.ipac.caltech.edu/data/Planck/release_2/ancillary-data/) .
- [114] B. D. Fields, *Ann. Rev. Nucl. Part. Sci.* **61**, 47 (2011) [arXiv:1203.3551 [astro-ph.CO]].
- [115] J. C. Howk, N. Lehner, B. D. Fields and G. J. Mathews, *Nature* **489**, 121 (2012) [arXiv:1207.3081 [astro-ph.CO]].
- [116] F. Hoyle, *Astrophys. J. Suppl.* **1**, 121 (1954).
- [117] P. D. O'Malley, D. W. Bardayan, A. S. Adekola, S. Ahn, K. Y. Chae, J. A. Cizewski, S. Graves and M. E. Howard *et al.*, *Phys. Rev. C* **84**, 042801 (2011).
- [118] O. S. Kirsebom and B. Davids, *Phys. Rev. C* **84**, 058801 (2011) [arXiv:1109.4690 [astro-ph.CO]].

- [119] M. W. Paris, G. M. Hale, A. C. Hayes-Sterbenz and G. Jungman, arXiv:1304.3153 [nucl-th].
- [120] F. Hammache, A. Coc, N. de Srville, I. Stefan, P. Roussel, S. Ancelin, M. Assi and L. Audouin *et al.*, Phys. Rev. C **88**, no. 6, 062802 (2013) [arXiv:1312.0894 [nucl-ex]].
- [121] J. R. Ellis, K. A. Olive and E. Vangioni, Phys. Lett. B **619** (2005) 30 [astro-ph/0503023]; M. Kusakabe, M. K. Cheoun and K. S. Kim, Phys. Rev. D **90**, no. 4, 045009 (2014) [arXiv:1404.3090 [astro-ph.CO]]; A. Coc, M. Pospelov, J. P. Uzan and E. Vangioni, Phys. Rev. D **90**, no. 8, 085018 (2014) [arXiv:1405.1718 [hep-ph]].
- [122] V. F. Shvartsman, Pisma Zh. Eksp. Teor. Fiz. **9**, 315 (1969) [JETP Lett. **9**, 184 (1969)];
- [123] G. Steigman, D. N. Schramm and J. E. Gunn, Phys. Lett. B **66**, 202 (1977); J. M. Yang, D. N. Schramm, G. Steigman and R. T. Rood, Astrophys. J. **227**, 697 (1979).
- [124] J. M. Yang, M. S. Turner, G. Steigman, D. N. Schramm and K. A. Olive, Astrophys. J. **281**, 493 (1984); G. Steigman, K. A. Olive, D. N. Schramm and M. S. Turner, Phys. Lett. B **176**, 33 (1986).
- [125] K. A. Olive, D. N. Schramm, G. Steigman and T. P. Walker, Phys. Lett. B **236**, 454 (1990); K. A. Olive and G. Steigman, Phys. Lett. B **354**, 357 (1995) [hep-ph/9502400].
- [126] C. J. Copi, D. N. Schramm and M. S. Turner, Phys. Rev. D **55** (1997) 3389 [astro-ph/9606059]; K. A. Olive and D. Thomas, Astropart. Phys. **7** (1997) 27 [hep-ph/9610319]; K. A. Olive and D. Thomas, Astropart. Phys. **11**, 403 (1999) [hep-ph/9811444].
- [127] E. Lisi, S. Sarkar and F. L. Villante, Phys. Rev. D **59**, 123520 (1999) [hep-ph/9901404].
- [128] S. Burles, K. M. Nollett, J. W. Truran and M. S. Turner, Phys. Rev. Lett. **82**, 4176 (1999) [astro-ph/9901157].
- [129] G. Mangano and P. D. Serpico, Phys. Lett. B **701**, 296 (2011) [arXiv:1103.1261 [astro-ph.CO]].
- [130] R. A. Alpher, H. Bethe and G. Gamow, Phys. Rev. **73**, 803 (1948); G. Gamow, Phys. Rev. **74**, 505 (1948); G. Gamow, Nature **162**, 680 (1948); R. Alpher, and R. Herman, Phys. Rev. **74**, 1737 (1948).
- [131] K. M. Nollett and G. P. Holder, arXiv:1112.2683 [astro-ph.CO].
- [132] E. Di Valentino, C. Gustavino, J. Lesgourgues, G. Mangano, A. Melchiorri, G. Miele and O. Pisanti, Phys. Rev. D **90**, no. 2, 023543 (2014) [arXiv:1404.7848 [astro-ph.CO]].
- [133] K. Sigurdson and S. R. Furlanetto, Phys. Rev. Lett. **97**, 091301 (2006) [astro-ph/0505173].